

1 **Magnesium (Mg/Ca,  $\delta^{26}\text{Mg}$ ), boron (B/Ca,  $\delta^{11}\text{B}$ ), and calcium ( $[\text{Ca}^{2+}]$ )**  
2 **geochemistry of *Arctica islandica* and *Crassostrea virginica***  
3 **extrapallial fluid and shell under ocean acidification**

4 Blanca Alvarez Caraveo<sup>1,2</sup>, Maxence Guillermic<sup>1,2,3</sup>, Alan Downey-Wall<sup>4</sup>, Louise P. Cameron<sup>4</sup>, Jill N.  
5 Sutton<sup>5</sup>, John A. Higgins<sup>6</sup>, Justin B. Ries<sup>4</sup>, Katie Lotterhos<sup>4</sup>, Robert A. Eagle<sup>1,2</sup>

6 <sup>1</sup>Atmospheric and Oceanic Sciences Department, University of California, Los Angeles, Math Sciences Building, 520  
7 Portola Plaza, Los Angeles, CA 90095, USA

8 <sup>2</sup>Center for Diverse Leadership in Science, Institute of the Environment and Sustainability, University of California, Los  
9 Angeles, LaKretz Hall, 619 Charles E Young Dr E no. 300, Los Angeles, CA 90024, USA

10 <sup>3</sup>Earth, Planetary and Space Sciences, Department, University of California, Los Angeles, Los Angeles, CA 90095, USA

11 <sup>4</sup> Department of Marine and Environmental Sciences, Marine Science Center, Northeastern University, 430 Nahant Rd,  
12 Nahant, MA 01908, USA

13 <sup>5</sup> Université de Brest, UMR 6539 CNRS/UBO/IRD/Ifremer, LEMAR, IUEM, 29280, Plouzané, France

14 <sup>6</sup> Department of Geosciences, Princeton University, Guyot Hall, Princeton NJ 08544, USA

15

16 *Correspondence to:* Blanca Alvarez Caraveo (alvarezblanca@ucla.edu) and Robert Eagle (robeagle@ucla.edu)

17 **Abstract.** The geochemistry of biogenic carbonates has long been used as proxies to record changing seawater parameters.  
18 However, the effect of ocean acidification on seawater chemistry and organism physiology could impact isotopic signatures  
19 and how elements are incorporated into the shell. In this study, we investigated the geochemistry of three reservoirs  
20 important for biomineralization - seawater, the extrapallial fluid (EPF), and the shell - in two bivalve species, *Crassostrea*  
21 *virginica* and *Arctica islandica*. Additionally, we examined the effects of three ocean acidification conditions (ambient: 500  
22 ppm CO<sub>2</sub>, moderate: 900 ppm CO<sub>2</sub>, and high: 2800 ppm CO<sub>2</sub>) on the geochemistry of the same three reservoirs for *C.*  
23 *virginica*. We present data on calcification rates, EPF pH, measured elemental ratios (Mg/Ca, B/Ca), and isotopic signatures  
24 ( $\delta^{26}\text{Mg}$ ,  $\delta^{11}\text{B}$ ). In both species, comparisons of seawater and EPF Mg/Ca and B/Ca,  $[\text{Ca}^{2+}]$ , and  $\delta^{26}\text{Mg}$  indicate that the EPF  
25 has a distinct composition that differs from seawater. Shell  $\delta^{11}\text{B}$  did not faithfully record seawater pH and  $\delta^{11}\text{B}$ -calculated pH  
26 values were consistently higher than pH measurements of the EPF with microelectrodes, indicating that the shell  $\delta^{11}\text{B}$  may  
27 reflect a localized environment within the entire EPF reservoir. In *C. virginica*, EPF Mg/Ca and B/Ca, as well as absolute  
28 concentrations of Mg<sup>2+</sup>, B, and  $[\text{Ca}^{2+}]$ , were all significantly affected by ocean acidification, indicating that OA affects the  
29 physiological pathways regulating or storing these ions, an observation that complicates their use as proxies. Reduction in  
30 EPF  $[\text{Ca}^{2+}]$  may represent an additional mechanism underlying reduction in calcification in *C. virginica* in response to  
31 seawater acidification. The complexity of dynamics of EPF chemistry suggest boron proxies in these two mollusc species are

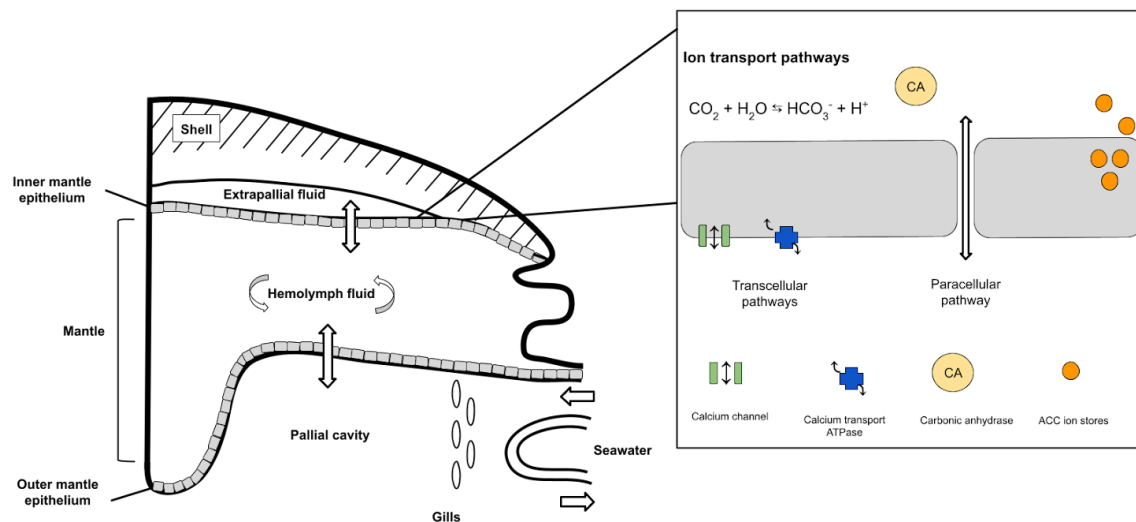
not straightforwardly related to seawater pH, but ocean acidification does lead to both a decrease in microelectrode pH and boron-isotope-based pH, potentially showing applicability of boron isotopes in recording physiological changes. Collectively, our findings show that bivalves have high physiological control over the internal calcifying fluid, which presents a challenge to using boron isotopes for reconstructing seawater pH.

## 1 Introduction

The elemental geochemistry of marine biogenic carbonate shells is widely used to track and reconstruct environmental change (e.g. Broecker and Peng, 1982; Elderfield, 2006). The incorporation of elements within the skeleton of marine calcifiers has been shown to be correlated with different environmental parameters, such as temperature (Dunbar et al., 1994, Alibert and McCulloch 1997) and pH (e.g. Hemming and Hanson, 1992; Hönisch et al., 2004; McCulloch et al., 2018). However, ~~it has long been recognised that~~ elemental and isotopic signatures of biogenic carbonate deviate from inorganic carbonate grown under the same conditions, complicating the use and interpretation of these theoretical models for paleo-reconstructions (e.g. Urey, 1951; Craig, 1953; ~~reviewed by~~ Weiner and Dove, 2003). “Vital effects” are ~~the~~ physiological processes that alter the geochemistry of biominerals and consequently offset the environmental signal incorporated in biogenic carbonates, ~~termed “vital effects” (Urey, 1951)~~ which includes the different biomineralization strategies that can modify the chemistry of the calcification fluid (Urey, 1951; Weiner and Dove, 2003). For organisms to calcify, a semi-isolated calcification space will be, to varying degrees, separated from seawater for supersaturation to be achieved in support of calcification (Weiner and Dove, 2003). ~~The intracellular calcification, biominerals can be formed within cells using specialized vesicles or vacuoles, whereas in extracellular cases, calcification may occur on an organic matrix template, with ions transported as necessary for crystal nucleation to occur (Weiner and Dove, 2003; Addadi et al., 2006; reviewed by Gilbert et al., 2022).~~ Additionally, the geochemistry of the calcification fluid can be altered due to differing degrees of isolation from the parent fluid, seawater, as well as the modulation of the calcification fluid chemistry via different methods of passive or active ion transport to the site of calcification (Weiner and Dove 2003; McCulloch et al., 2017; Sutton et al., 2018; Liu et al., 2020). A mechanistic understanding of such vital effects is desirable for the accurate interpretation of geochemical proxies preserved in the shells of these organisms.

Molluscs have long been recognized as valuable archives for climate reconstructions, given their annual resolution growth bands, long lifespans, and wide geographic distributions (Gibson et al., 2001; Immenhauser et al., 2016; Peharda et al., 2021). ~~However, it is also well established that mollusc shells carbonates can also exhibit express significant vital effects for in different many geochemical parameters (Schöne, 2008).~~ Several different elemental systems like boron (B) and magnesium ( $Mg^{2+}$ ) can give valuable information about the seawater bivalves precipitate their shells in or even in internal calcification fluid they precipitate their shells from. For example, shell B/Ca has been shown to be correlated to internal fluid pH in *Mytilus edulis* (Heinemann, 2012) and *Mercenaria mercenaria* (Ulrich et al., 2021), which can be useful in understanding the internal carbonate chemistry within the calcification fluid. Shell  $\delta^{11}B$  is used as a ~~proxys proxy~~ proxy for

seawater pH in foraminifera (Foster and Rae, 2016) and corals (McCulloch et al., 2017; Eagle et al., 2022), but seems to be relatively insensitive to vital effects in many molluscs. Shell  $\delta^{11}\text{B}$  is offset from theoretical pH calculations examined, including bivalves like *Mytilus edulis* (Heinemann et al., 2012; Liu et al., 2020), *Mercenaria mercenaria* (Liu et al., 2020), and *Crassostrea virginica* (Heinemann et al., 2012; Foster and Rae, 2016; McCulloch et al., 2017; Liu et al., 2020; Eagle et al., 2022). Shell B/Ca has been shown to be correlated to internal fluid pH in *Mytilus edulis* (Heinemann, 2012) and *Mercenaria mercenaria* (Ulrich et al., 2021), but relationships to seawater pH were less clear. Molluscs  $\delta^{11}\text{B}$  does not faithfully record seawater pH, but rather the pH of the extrapallial fluid (EPF) which is the discrete fluid from which ions are sourced for calcification (Gilbert et al., 2022). Shell Reported Mg/Ca are widely used as a temperature proxies in bivalves many marine calcifiers (Wannamaker et al., 2008; Schöne et al., 2011), however it is also long established that molluscs can regulate and actively exclude  $[\text{Mg}^{2+}]$  from their shells (Lorens and Bender, 1977; Planchon et al., 2013), showing that biological regulation of the internal biocalcification and the parent fluids for shell formation can have a strong influence on Mg-based geochemical proxies. Additionally Mg<sup>2+</sup> isotope analyses can potentially inform the  $[\text{Mg}^{2+}]$  transport process in molluscs. Although few Mg isotope studies of molluscs have been done, a study by Planchon et al. (2013) investigated the  $\delta^{26}\text{Mg}$  of across *Ruditapes philippinarum* tissues, shell, and EPF fluid reservoirs and found that seawater and extrapallial fluid Mg magnesium isotopic signatures were similar, suggesting that seawater is the source of  $[\text{Mg}^{2+}]$  ions within the extrapallial fluid. Additionally, they Planchon et al. (2013) found that Mg signatures of some specimen within the shell varied between specimens and were either in line with or deviated from inorganically precipitated aragonite, suggesting an ability for some clams to physiologically alter or regulate  $[\text{Mg}^{2+}]$  within the extrapallial fluid (Planchon et al., 2013).



f 01

82

83

84 Figure 1. Schematic of a bivalve cross section showing the flow of between biomineralization ion reservoirs. The box on the  
 85 right shows a zoomed in schematic across the inner mantle epithelium cells that show transcellular and paracellular ion  
 86 transport pathways in and between epithelial cells. Figure adapted from Planchon et al. (2013) and Zhao et al. (20176).¶¶

87 ¶¶

88

89 Understanding the elemental composition and isotope signaturesstructure of mollusc tissues, internal fluid reservoirs,  
 90 mechanisms of calcification and ion transport to the site of calcification is critical to understanding these vital effects (Fig 1).  
 91 It may also give insight into the sensitivity of bivalves to CO<sub>2</sub> induced ocean acidification, a major environmental challenge  
 92 to ocean ecosystems and commercial shellfish fisheries (Gazeau et al., 2013; Stewart-Sinclair et al., 2020). Typically,  
 93 bivalves are amongst the more sensitive group of marine calcifier species to acidification (Ries et al., 2009; Kroeker et al.,  
 94 2011).¶¶

95

The bivalve mollusc extrapallial fluid (EPF) is an internal fluid reservoir physically semi-separated from seawater that circulates in the pallial cavity, between the outer mantle organ epithelium (OME) and shell (Wilbur and Saleuddin, 1983). Seawater enters the pallial cavity when valves are open, then the internal hemolymph fluid circulates within the organs of the mollusc and finally can also be transported across the mantle to the EPF (Table 1; Zhao et al., 2018a). Bivalve mollusc shell calcification is thought to occur at the interface of the EPF and growing shell where the ions for calcification interact with organic matrices, such as polypeptide molecules (Crenshaw, 1972; Wheeler and Sikes, 1984; Wilbur and Bernhardt, 1984; Addadi, 2006) and proteins within the EPF that act as a scaffolding template for nucleation and are important in the calcification process (Crenshaw, 1972; Wilbur and Bernhardt, 1984; Addadi, 2006). Additionally, molluscs have been shown to calcify through a transient amorphous calcium carbonate precursor phase in which disordered calcium carbonate crystals can be stored and then transported to the calcification front (Addadi, 2003; Immenhauser et al., 2016), which can act as another source of potential geochemical vital effects. Therefore, it is expected that EPF chemistry will differ from seawater and that knowledge of EPF geochemistry may inform our knowledge of vital effects in bivalve molluscs. ¶

Unlike the calcifying fluid reservoirs in most organisms, bivalve EPF has a large enough volume that it can be directly sampled, allowing for direct measurements of the reservoir to compare with seawater geochemistry and elucidate in situ changes in EPF chemistry. A foundational study by Crenshaw (1972) found that, in three mollusc species, the EPF calcification fluid had a different chemical composition and pH from seawater and from the mollusc hemolymph fluid (Crenshaw et al., 1972). Crenshaw, (1972) reported that EPF pH was significantly lower than seawater pH, that cationic compositions of the EPF could also differ from seawater, and that the total carbon C (including all species of dissolved inorganic carbon) of the EPF was higher than that of seawater. Additionally, Crenshaw (1972) also showed that EPF calcium concentration and pH co-varied significantly over time during the opening and closing of valves, or the ventilation cycle. When valves are closed pH is lower and calcium concentration higher, resulting from dissolution of shell material and return of calcium to the EPF (Crenshaw, 1972). A previous study on the king scallop, *Pecten maximus*, by Cameron et al. (2019) showed that EPF pH was lower than seawater and also depended on seawater  $p\text{CO}_2$ ,  $\text{pCO}_2$  and temperature. Additionally, Ramesh et al., (2017) used reported, using a microelectrode approach to show, that pH and  $[\text{CO}_3^{2-}]$  were elevated proximal to the growing shell in larval *Mytilus edulis* shells. This result using microelectrode suggests a potential difference in pH between the bulk EPF and the pH close to the site of calcification. In the quahog *Arctica islandica*, Stemmer et al. (2019) reported synchronous short-term fluctuations in EPF  $[\text{Ca}^{2+}]$  and the pH at the outer mantle epithelium surface, providing further support that the extrapallial fluid of molluscs is a discrete fluid under biological control. They attributed this to active ion pumping across mantle epithelial cells, which created significant differences between carbonate saturation and pH of the bulk EPF and the EPF close to the outer mantle epithelium. Understanding the elemental composition and isotope signatures of mollusc tissues, internal fluid reservoirs, mechanisms of calcification and ion transport to the site of calcification is critical to understanding these vital effects. It may also give insight into the sensitivity of bivalves to  $\text{CO}_2$ -induced ocean acidification, a major environmental challenge for bivalves, which are typically amongst the more sensitive group of marine calcifier species to acidification (Ries et al., 2009; Kroecker et al., 2011; Gazeau et al., 2013; Stewart-Sinclair et al., 2020).

Boron proxies utilise boron speciation and isotope fractionation in seawater to reconstruct pH and  $[\text{CO}_3^{2-}]$  of seawater from the chemistry of calcium carbonate shells (Hemming and Hanson, 1992; Hönisch et al., 2004). In seawater, the speciation of boric acid  $[\text{B}(\text{OH})_3]$  and borate ion  $[\text{B}(\text{OH})_4^-]$  varies as a function of pH (Hemming and Hanson 1992). In addition to the pH dependence of their relative abundances, the boron proxy also makes use of a large isotopic fractionation between the two boron species (Klochko et al., 2006; Nir et al., 2015). A key assumption of the proxy is that boron, in the form of borate ion, is the predominant form incorporated into the crystal lattice of calcite via carbonate ion substitution during the precipitation of calcium carbonate (Hemming and Hanson 1992). The  $\delta^{11}\text{B}$  of the carbonate ( $\delta^{11}\text{B}_{\text{CaCO}_3}$ ) should then, in theory, reflect the boron isotopic composition of the borate ion in seawater ( $\delta^{11}\text{B}_{\text{CaCO}_3}$ ). Accurate reconstruction of seawater pH can then be achieved using specific empirical relationships between the  $\delta^{11}\text{B}_{\text{CaCO}_3}$  and  $\delta^{11}\text{B}_{\text{CaCO}_3}$ , which can in turn be used to determine pH. The marine boron system is also utilized in the development of B/Ca proxies, which utilize the substitution of boron for  $[\text{CO}_3^{2-}]$  in the crystal lattice and the relationship between the partition coefficient ( $K_D$ ), B/Ca, and  $[\text{CO}_3^{2-}]$  to create a proxy for  $[\text{CO}_3^{2-}]$  of seawater or calcifying fluid (reviewed by DeCarlo et al., 2018). Using the exchange reactions for the substitution of boron during aragonite or calcite precipitation, the founding assumption of the proxy is that B/Ca of the shell can be used to calculate the  $[\text{CO}_3^{2-}]$  of the solution from which the aragonite or calcite precipitated. Inorganic aragonite precipitation experiments have validated the B/Ca proxy by allowing for the calculation of the partition coefficient ( $K_D$ ) between aragonite and seawater and fitting of experimental B/Ca data (Mavromatis et al., 2015; Holcomb et al., 2016; Allison 2017; reviewed by DeCarlo et al., 2018). However the B/Ca proxy also has limitations, as it has only been developed for aragonite samples and because of remaining unresolved differences in the formulation of the  $K_D$ , exchange reactions, and fitting of B/Ca experimental data between studies (Allison et al., 2017; McCulloch et al., 2017; DeCarlo et al., 2018; Holcomb et al., 2016). Together, both  $\delta^{11}\text{B}$  ( $\text{pH}_{\text{CT}}$ ) and B/Ca ( $[\text{CO}_3^{2-}]$ ) proxies can be used to constrain the full carbonate system of the calcifying medium (DeCarlo et al., 2018).

Vital effects of the  $\delta^{11}\text{B}$  can be species-specific and, in the case of foraminifera, vital effects are relatively minor (Hönisch et al., 2004; Foster and Rae, 2016). However, other calcifying organisms, such as corals, coralline red algae, and molluscs, show significant  $\delta^{11}\text{B}$  deviations from relationships predicted from theoretical calculations (e.g., Donald et al., 2017; Schoepf et al., 2017; McCulloch et al., 2018; Sutton et al., 2018; Anagnostou et al., 2019; Liu et al., 2020). There are different theories to explain the divergence of  $\delta^{11}\text{B}$  from the seawater theoretical model. It is hypothesized for some taxa that  $\delta^{11}\text{B}$  may not faithfully record seawater pH, but rather the pH of the discrete fluid from which ions are sourced for calcification that may be isolated or semi-isolated from seawater (Gilbert et al., 2022). Previous work on corals has used the boron proxy analyses, along with other approaches, to probe internal carbonate chemistry of the calcification fluid (Ries, 2011; Holcomb et al., 2014; Guillerme et al., 2021; Cameron et al., 2022; Eagle et al., 2022; Allison et al., 2023). All approaches, both geochemical and physiological, indicate that corals elevate the pH and  $[\text{CO}_3^{2-}]$  of their calcifying fluid to induce calcification, but this mechanism is sensitive to ocean acidification and has yet to be fully understood (Liu et al., 2020; Guillerme et al., 2021; Cameron et al., 2022; Eagle et al., 2022).

Beyond corals, few taxa have been studied using combined geochemical tracer work to determine the chemistry of calcification fluid pools and sources of ions to the calcification front. Work by Sutton et al. (2018) noted that  $\delta^{11}\text{B}$  values in urchin spines were lower than seawater borate  $\delta^{11}\text{B}$ . Stumpp et al. (2013) showed that the internal pH of sea urchin larvae was typically lower than seawater pH. Short et al. (2015), Donald et al. (2017), Anagnostou et al. (2019), and Liu et al. (2020) found high  $\delta^{11}\text{B}$  in calcite produced by coralline algae, which is potentially consistent with elevation of calcifying fluid pH in support of calcification either through enzymatic proton removal and/or photosynthetically driven removal of dissolved inorganic carbon from the calcifying fluid. To date, one study has investigated the B/Ca and  $\delta^{11}\text{B}$  of shell and EPF of the bivalve *Mytilus edulis* (Heinemann et al., 2012).

The mollusc extrapallial fluid is an attractive target to investigate geochemical vital effects because not only can it be probed with electrodes, like for corals, but it can also be extracted and analyzed. In this study, we investigate the  $\delta^{11}\text{B}$ , B/Ca,  $\delta^{26}\text{Mg}$ , and Mg/Ca in extracted extrapallial fluid and aragonite shell of the quahog, *Arctica islandica*, and the calcite shell of the eastern oyster, *Crassostrea virginica*. This allows for the investigation of the tripartite fractionation between seawater, extrapallial fluid, and shell. Individuals were kept in controlled laboratory experiments, with extrapallial fluid pH determined with microelectrodes, and other physiological parameters, such as calcification rate and tissue production, determined by conventional methods (Downey-Wall et al., 2020). Additionally, in order to examine if elemental ratios and isotopic signatures can be impacted under ocean acidification, specimens of *C. virginica* were also cultured in three different treatments of  $\text{pCO}_2$ : ambient, moderate and high ocean acidification conditions. Geochemical analysis of the seawater, shell, and extrapallial fluid thereby allow novel insights into the transport of ions from seawater to the extrapallial fluid, and the fractionation of isotopes and elements between the extrapallial fluid and shell under both control and acidified conditions.

## 2 Materials and Methods

### 2.1 Experimental Conditions

Adult *A. islandica* specimens were collected from Beals Island, Maine, USA (44°31'11"N, 67°36'54"W) in March 2018, transferred to Northeastern University's Marine Science Center, and maintained in the lab until March 2019. For *A. islandica*, seawater was maintained at a pH of  $7.93 \pm 0.09$ , temperature of  $9 \pm 1$  °C, and salinity of 35 in the control conditions (Cameron 2020).

A detailed explanation of the collection and culturing of *C. virginica* is outlined in Downey-Wall et al. (2020). Adult *C. virginica* specimens were collected from three intertidal sites on Plum Island Sound, Massachusetts, USA (Site 1, 42°45'6" N, 70°50'13" W; Site 2, 42°43'31" N, 70°51'18" W; Site 3, 42°40'43" N, 70°48'49" W) in April 2017 and transferred to Northeastern University's Marine Science Center. The average *C. virginica* shell length was  $9.23 \pm 2.4$  cm and shell width



was  $5.4 \pm 0.8$  cm ( $n=107$ ). A detailed explanation of the collection and culturing of *C. virginica* and *A. islandica* is outlined in Downey Wall et al. (2020). Specimens were acclimated to laboratory conditions for 33 days and then transferred to experimental tanks. For the ambient experiment, seawater salinity and temperature, and pH (total scale) were monitored and maintained throughout the experiment. *C. virginica* seawater was maintained at a pH of  $8.01 \pm 0.08$ , temperature of  $18.2 \pm 1$  °C, and salinity of 31 psu for the calcitic oyster *C. virginica*. Seawater was maintained at a pH of  $7.93 \pm 0.09$ , temperature of  $18.2 \pm 1$  °C, and salinity of 35 psu for the aragonitic clam *A. islandica* in the control conditions (Downey Wall et al., 2020). For the *C. virginica* ocean acidification experiment, seawater temperature and salinity were maintained the same as above and pCO<sub>2</sub> for each treatment was set to ¶

Adult *A. islandica* specimens were collected from Beals Island, Maine, USA ( $44^{\circ}31'11''$ N,  $67^{\circ}36'54''$ W) in March 2018, transferred to Northeastern University's Marine Science Center, and maintained in the lab until March 2019. Seawater was maintained at a pH of  $7.93 \pm 0.09$ , temperature of  $18.2 \pm 1$  °C, and salinity of 35 psu for the aragonitic clam *A. islandica* in the control conditions (Downey Wall et al., 2020). ¶

Adult *C. virginica* specimens were collected from three intertidal sites on Plum Island Sound, Massachusetts, USA (Site 1,  $42.75$  N,  $70.84$  E; Site 2,  $42.73$  N,  $70.86$  E; Site 3,  $42.68$ ,  $70.81$ ) and transferred to Northeastern University's Marine Science Center. Following a 33-day period of acclimation to laboratory conditions, *C. virginica* oysters from each collection site were exposed to control (mean pCO<sub>2</sub> pCO<sub>2</sub>  $\pm$  SE =  $570 \pm 14$  ppm;  $\Omega_{\text{calcite}} = 2.95 \pm 0.30$ ), moderate OA ( $990 \pm 29$  ppm,  $\Omega_{\text{calcite}} = 1.93 \pm 0.32$ ), or high OA ( $2912 \pm 59$  ppm,  $\Omega_{\text{calcite}} = 0.75 \pm 0.09$ ) treatments. Target pCO<sub>2</sub> pCO<sub>2</sub> treatment was achieved by mixing compressed pCO<sub>2</sub> CO<sub>2</sub> and compressed ambient air using solenoid-valve-controlled mass flow controllers at flow rates that target pCO<sub>2</sub> pCO<sub>2</sub> conditions. The treated seawater was introduced to the flow-through aquaria at a rate of  $150 \text{ mL min}^{-1}$ . For the acidification experiment, Tank salinity, temperature, and DIC and TA were measured for the duration of the experiment and used to calculate pH (total scale),  $\Omega_{\text{calcite}}$ , [CO<sub>3</sub><sup>2-</sup>], [HCO<sub>3</sub><sup>-</sup>], [CO<sub>2</sub>], and pCO<sub>2</sub> pCO<sub>2</sub> of each tank using CO2SYS version 2.1 (Pierrot et al. 2011; see Downey-Wall et al. 2020). Measured and calculated seawater parameters are reported in Table 1. Oysters were fed 1% Shellfish Diet 1800® twice daily following best practices outlined in Helm and Bourne (2004).

219

	Control <i>A. islandica</i>	Control <i>C. virginica</i>	Moderate OA <i>C. virginica</i>	High OA <i>C. virginica</i>
	Measured seawater parameters			
pH (total scale)	$7.93 \pm 0.09$	$8.01 \pm 0.08$	$7.75 \pm 0.07$	$7.29 \pm 0.11$
DIC (µmol/kg)	n/d	$1966 \pm 44$	$1998 \pm 212$	$2177 \pm 160$
TA (µmol/kg)	n/d	$2120 \pm 46$	$2120 \pm 42$	$1511 \pm 40$



Mg/Ca (mol/mol)	5.13 ± 0.07	5.15 ± 0.07	5.23 ± 0.06	5.12 ± 0.03
δ <sup>26</sup> Mg (‰)	-0.82 ± 0.06 ‰	-0.77 ± 0.01	-0.82 ± 0.03	-0.76 ± 0.09
B/Ca (mol/mol)	41.75 ± 1.52	41.66 ± 1.07	43.08 ± 2.9	42.11 ± 1.8
δ <sup>11</sup> B (‰)	39.88 ± 0.13	40.29 ± 0.33	39.39 ± 0.33	39.82 ± 0.33
Calculated seawater parameters				
pCO <sub>2</sub> (ppm)	n/d	570 ± 90	990 ± 173	2912 ± 373
[CO <sub>3</sub> <sup>2-</sup> ] (μM)	n/d	120 ± 12	79 ± 13	31 ± 4
Ω <sub>Calcite</sub>	n/d	2.95 ± 0.30	1.93 ± 0.32	0.75 ± 0.09
Ω <sub>Aragonite</sub>	n/d	1.89 ± 0.19	1.24 ± 0.21	0.48 ± 0.06
δ <sup>11</sup> B-calculated pH (total scale)	7.76 ± 0.07	8.12 ± 0.09	8.06 ± 0.10	8.01 ± 0.08
ΔpH <sub>SW</sub> -δ <sup>11</sup> B <sub>pH</sub>	0.17	0.64	0.77	0.88

**Table 1.** Seawater carbonate chemistry parameters (pH, DIC, TA, Ω, δ<sup>11</sup>B-calculated EPF pH, and ΔpH) for both *C. virginica* and *A. islandica* under control conditions and *C. virginica* for OA conditions.. Seawater geochemical parameters (Mg/Ca, δ<sup>26</sup>Mg, B/Ca, δ<sup>11</sup>B) for both *C. virginica* and *A. islandica* under control conditions and *C. virginica* for OA conditions. Parameters that were unable to be not measured due to insufficient sample size or unable to be calculated are marked with ‘n/d.’

	Control <i>A. islandica</i>	Control <i>C. virginica</i>	Moderate OA <i>C. virginica</i>	High OA <i>C. virginica</i>
Measured seawater parameters				
pH (total scale)	7.93 ± 0.09	8.01 ± 0.08	7.75 ± 0.07	7.29 ± 0.11
DIC (μmol/kg)	n/d	1966 ± 44	1998 ± 212	2177 ± 160
TA (μmol/kg)	n/d	2120 ± 46	2120 ± 42	1511 ± 40
Mg/Ca (mol/mol)	5.13 ± 0.07	5.15 ± 0.07	5.23 ± 0.06	5.12 ± 0.03

$\delta^{26}\text{Mg}$ (‰)	0.82 ± 0.06 ‰	0.77 ± 0.01	0.82 ± 0.03	0.76 ± 0.09
B/Ca (mol/mol)	41.75 ± 1.52	41.66 ± 1.07	43.08 ± 2.9	42.11 ± 1.8
$\delta^{11}\text{B}$ (‰)	39.88 ± 0.13	40.29 ± 0.33	39.39 ± 0.33	39.82 ± 0.33
		Calculated seawater parameters		
$p\text{CO}_2$ (ppm)	n/d	570 ± 90	990 ± 173	2912 ± 373
$[\text{CO}_3^{2-}]$ (μM)	n/d	120 ± 12	79 ± 13	31 ± 4
$\Omega_{\text{Calcite}}$	n/d	2.95 ± 0.30	1.93 ± 0.32	0.75 ± 0.09
$\Omega_{\text{Aragonite}}$	n/d	1.89 ± 0.19	1.24 ± 0.21	0.48 ± 0.06
$\delta^{11}\text{B}$ calculated	7.76 ± 0.07	8.12 ± 0.09	8.06 ± 0.10	8.01 ± 0.08
pH (total scale)				
$\Delta\text{pH}_{\text{sw}} \delta^{11}\text{B}_{\text{pH}}$	0.17	0.64	0.77	0.88

Table 1. Seawater and extrapallial fluid carbonate chemistry parameters (pH, DIC, TA,  $\Omega$ ,  $\delta^{11}\text{B}$ -calculated EPF pH, and  $\Delta\text{pH}$ ) for both *C. virginica* and *A. islandica* under control conditions and *C. virginica* for OA conditions.. Seawater, extrapallial fluid, and shell geochemical parameters (Mg/Ca,  $\delta^{26}\text{Mg}$ , B/Ca,  $\delta^{11}\text{B}$ ) for both *C. virginica* and *A. islandica* under control conditions and *C. virginica* for OA conditions. Parameters that were unable to be not measured due to insufficient sample size or unable to be calculated are marked with ‘n/d.’

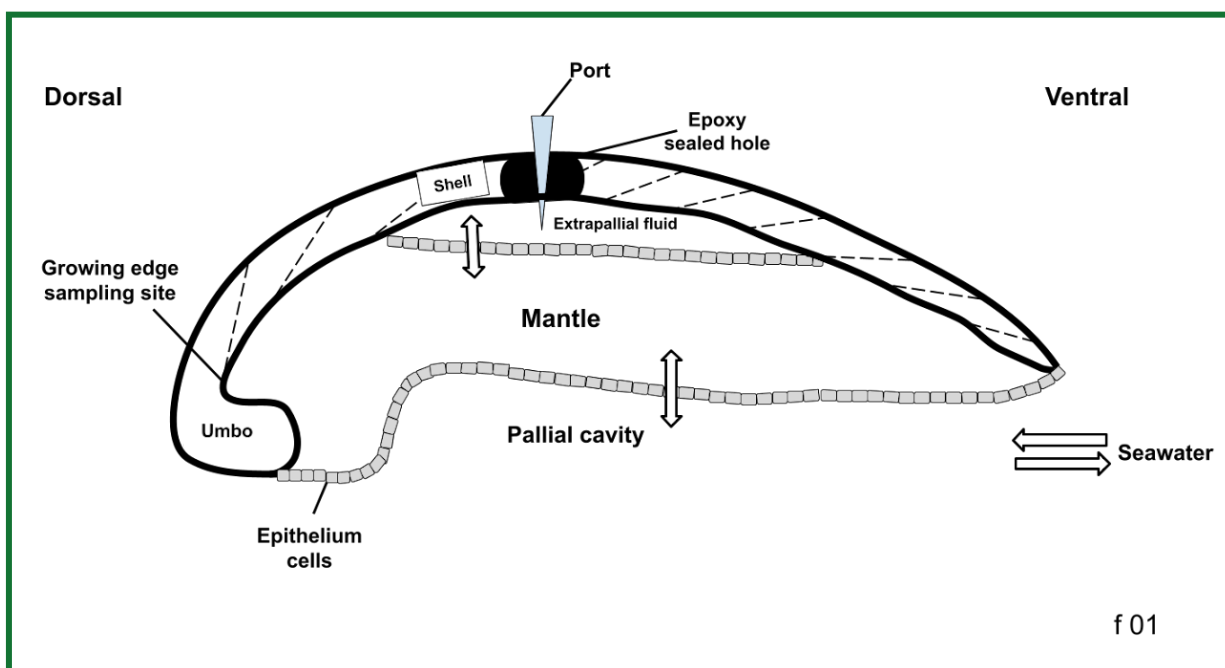
## 2.2 Calcification rate measurements

Net calcification rate for *C. virginica* specimen (n=35) was calculated in Downey-Wall et al., (2020) using the buoyant weighing technique. Buoyant weight was measured by submerging oysters in a 27.65 liter tank (48 cm long, 24 cm wide and 24 cm deep) filled with seawater. Specimens were placed on a bottom-loading scale (Cole Parmer Symmetry S-PT 413E, precision= 0.001 g) and weighed three times. At the end of the experiment, an empirical linear relationship was created between buoyant weight and dry shell weight of shucked oysters following the same methodology in Ries et al., 2009. The residual mean squared error (RMSE) for the dry weight/buoyant weight model was 1.939 mg. Calcification was

238 calculated as the difference in calculated dry weight at the start and end of the experiment over the number of days. This  
239 number was then divided by the initial weight and multiplied by 100 to get the percent change in calcification. ¶¶  
240 ~~using the dry weight at the start and end of the experiment. Initial dry weight was measured at the start of exposure,~~  
241 ~~on day 33 or 34, after the acclimation period and then at the end of the experiment (Downey-Wall et al., 2020). Dry weight~~  
242 ~~was estimated from buoyant weight measurements using the linear relationship between oyster dry~~¶  
243 ~~weight and oyster buoyant weight derived empirically for oysters~~¶¶  
244 ~~investigated in the present study~~¶¶  
245 ~~The buoyant weight was measured on either day 50 or 80 and the final dry weight was derived using a linear~~  
246 ~~relationship between oyster dry weight and oyster buoyant weight following the method in (Ries et al., (2009). The dry~~  
247 ~~weight to buoyant weight linear model relationship was structured this way to be able to predict dry weight from buoyant~~  
248 ~~weight without destructively sampling an oyster. The residual mean squared error (RMSE) for the dry weight/buoyant weight~~  
249 ~~model was 1.939 mg.~~¶  
250 ¶

### 251 2.3 Extrapallial fluid sampling

252 Sampling of the extrapallial fluid (EPF) for both species was previously described in Downey-Wall et al. (2020).  
253 Briefly, a hole was drilled onto the shell to expose the EPF cavity, a port was inserted and sealed with epoxy to directly  
254 sample the EPF with a syringe and prevent seawater intrusion (Figure 1). Oysters recovered for 4 days before being  
255 transferred to experimental tanks for acclimation before the experiment. To sample the EPF, oysters were removed from the  
256 tanks and EPF was extracted by inserting a sterile 5 mL syringe with a flexible 18-gauge polypropylene tip through the port.  
257 EPF samples were stored in 2 mL microcentrifuge tubes and refrigerated at 6°C for further analysis. EPF pH (Total scale) of  
258 the EPF was measured directly after extraction using a micro-pH probe. EPF measurements were collected at the end of the  
259 experiment, on day 71, for *C. virginica* and day 14 for *A. islandica*. EPF pH diel variability was also explored by measuring  
260 EPF pH at 6 timepoints to produce time series for both species in a 24-hour period.



261

262 **Figure 1.** Schematic of a bivalve cross section from the dorsal to the ventral sides. Seawater enters the pallial cavity and ions  
 263 can diffuse or be transported across the mantle organ to the extrapallial fluid space. A hole was drilled through the top of the  
 264 shell into the extrapallial fluid space and sealed with epoxy following port insertion. Shell material was drilled on the inner  
 265 side of the growing edge of the shell to sample new growth.

## 266 2.4 Shell sampling

267 Following EPF extraction, ~~bivalves~~ ~~oysters~~ were shucked and cleaned in 90% ethanol. The cleaned shells were dried  
 268 at room temperature for 48 hours and sealed in plastic bags for analysis. Shells were cut into cross sections from the hinge to  
 269 the margin using a circular saw. Shells were rinsed with ethanol during sectioning to prevent mineralogical changes from  
 270 heat exposure. For skeletal geochemical and elemental ratio analysis, the inner (lamellar) layer of the oyster shell was gently  
 271 shaved with a diamond-tipped Dremel tool. Care was taken to ensure sampling the most recently deposited material right  
 272 near the growing edge of the bivalve, located below the umbo of the oyster shell (Figure 1). Cross sections showed growth  
 273 bands and aided in sampling the newest growth under experimental conditions. For *A. islandica*, we wanted to compare  
 274 ambient conditions, so new growth was not necessary to sample. ~~and~~ About 5 mg of ground powder was stored in sealed  
 275 microcentrifuge tubes.

## 276 2.4 Elemental ratio analysis

277 For the shells, about 2.5 mg of powder was sub-sampled from each specimen shell and cleaned with a 0.3 %  
278 hydrogen peroxide in 0.1 N sodium hydroxide solution to remove organic matter as described in Barker et al. (2003).  
279 Carbonate samples were dissolved in 1 N double-distilled HCl (see Guillermic et al., 2021, for details). Elemental ratios  
280 were measured on a Thermo Fisher Scientific Element XR HR-ICP-MS at the PSO (Plouzané, France) after Ca analyses on  
281 an Agilent ICP-AES Varian 710 at the University of California, Los Angeles (UCLA, Los Angeles, USA). Data quality and  
282 external reproducibility were maintained and quantified via repeated measurements of international standard JC<sub>P</sub>-1 during a  
283 particular session (Gutjahr et al., 2021). Typical measured concentrations of procedural blanks for the trace element analyses  
284 for sessions in which samples are diluted to 30 ppm Ca are  $^7\text{Li} < 3\%$ ,  $^{11}\text{B} < 4\%$ ,  $^{25}\text{Mg} < 0.1\%$ ,  $^{87}\text{Sr} < 0.1\%$ , and  $^{43}\text{Ca} < 0.1\%$ .  
285 Typical analytical uncertainties on the X/Ca elemental ratios are 0.3  $\mu\text{mol/mol}$  for Li/Ca, 21  $\mu\text{mol/mol}$  for B/Ca, 0.09  
286 mmol/mol for Mg/Ca, and 0.01 mmol/mol for Sr/Ca (2 SD, n = 28).

287 For EPF and seawater samples, 10  $\mu\text{L}$  of sample was added to 490  $\mu\text{L}$  of a solution of 0.1 N  $\text{HNO}_3$ /0.3 M HF.  
288 Mono-elemental solution of indium was added to reach a concentration of 1 ppb to monitor any matrix effect or drift of the  
289 instrument during a particular session. Standards were prepared by diluting an in-house seawater standard spiked with  
290 indium. International standards NRC-NASS-6 was used to ensure quality of the data.

## 291 2.5 Boron isotope analyses

292 Boron purification for the different samples was achieved via microdistillation following the method described in  
293 Guillermic et al. (2021) and originally developed by Gaillardet et al. (2001) and modified for Ca-rich matrix by Wang et al.  
294 (2010). Approximately 2.5-3.0 mg of oxidatively cleaned shell powders were dissolved in 1N HCl. For the EPF, 25  $\mu\text{L}$  of  
295 EPF was added to 40  $\mu\text{L}$  of 1N HCl. For the seawater, 50  $\mu\text{L}$  of concentrated HCl was added to 450  $\mu\text{L}$  of seawater. 60 $\mu\text{L}$  of  
296 each of the solutions was loaded for microdistillation. Boron isotopes were analyzed at the Pôle Spectrométrie Océan (PSO),  
297 Plouzané, on a Thermo Neptune inductively coupled plasma mass spectrometry (MC-ICP-MS) equipped with 10<sup>11</sup> Ohm  
298 Faraday cup.

299 The certified boron isotope liquid standard ERM© AE120 ( $\delta^{11}\text{B} = -20.2 \pm 0.6 \%$ , Vogl et al., and Rosner, 2011) was  
300 used to monitor reproducibility and drift during each session. Samples measured for boron isotopes in carbonates were  
301 typically run at 80 ppb B (~30 ng B per <0.5 mL), whereas samples of EPF and seawater were typically run at 150-200 ppb  
302 B (~150 ng B per mL). Sensitivity on  $^{11}\text{B}$  was 10 mV/ppb B (e.g., 10 mV for 1 ppb B) in wet plasma at 50  $\mu\text{L/min}$  sample  
303 aspiration rate. Procedural boron blanks ranged from 0.3 to 0.4 ng B and the acid blank during analyses was measured at 3  
304 mV on the  $^{11}\text{B}$ , indicating a total blank contribution of <2% of the sample signal with no memory effect within and across  
305 sessions. External reproducibility was ensured by the measurements of carbonate standard microdistilled at the same time as  
306 the samples. Results for the isotopic composition of the JC<sub>P</sub>-1 is  $\delta^{11}\text{B} = 24.67 \pm 0.28 \%$  (2 SE, n=41), within error of  
307 published values ( $24.36 \pm 0.45 \%$ , 2SD, Gutjahr et al., 2021).

## 308 2.6 Magnesium isotope analyses

309 Carbonate samples were dissolved in 0.1 N buffered acetic acid ammonium hydroxide solution over four hours in a  
310 sonicator. Samples were then centrifuged and aliquots of the supernatant were transferred into cleaned 15 mL centrifuge  
311 tubes. Aliquots of the bulk supernatants were then diluted ~30-fold and calcium and magnesium were separated and purified  
312 in different runs via a Thermo-Dionex ICS-5000+ ion chromatograph equipped with a fraction collector according to  
313 established methods outlined by Husson et al. (2015). EPF samples contained organics that obscured elution profiles, thus  
314 limiting the elemental yield and purification. Therefore, samples were digested on a hot plate in hydrogen peroxide and nitric  
315 acid to remove organics prior purification. Seawater and EPF samples were purified through the Thermo-Dionex ICS-5000+  
316 ion chromatograph using another elution method than for carbonate samples. Seawater and carbonate standards were also  
317 purified at the same time to ensure quality of the method.

318 Samples were then dried and then rehydrated in a solution of 2% nitric acid. Magnesium isotopic ratios were  
319 measured at Princeton University using a Thermo Neptune+ (MC-ICP-MS) spectrometer according to methods outlined in  
320 Higgins et al. (2018) and Ahm et al. (2021). Samples were introduced via an ESI Apex-IR sample introduction system.  
321 Magnesium isotope ratios ( $^{26}\text{Mg}/^{24}\text{Mg}$ ) were measured in low resolution mode, with every sample bracketed by the analysis  
322 of standards. Results are reported relative to the Dead Sea Magnesium-3 standard (DSM-3). Long term external precision on  
323 magnesium isotope results at the Higgins Lab (Princeton) was determined through repeated measurements of the  
324 Cambridge-1 standard ( $-2.59 \pm 0.07\text{‰}$ , 2 SD,  $n = 19$ ) and modern seawater ( $-0.82 \pm 0.14 \text{‰}$ , 2 SD,  $n = 21$ ) and is reported  
325 in Ahm et al. (2021). Measured standards during the analytical session are given for the Cambridge-1 standard ( $-2.60 \pm 0.20$   
326  $\text{‰}$ , 2 SD,  $n = 2$ ) and for modern seawater ( $-0.82 \pm 0.06 \text{‰}$ , 2 SD,  $n=2$ ).

## 327 2.7 Calculation of boron proxies and EPF carbonate chemistry

328 The use of boron proxies to reconstruct pH and  $[\text{CO}_3^{2-}]$  of the precipitating solution (i.e., the organism's calcifying  
329 fluid) is based upon boron speciation and fractionation in seawater (Hemming and Hanson, 1992; Hönisch et al., 2004). In  
330 seawater-type solutions, the speciation of boric acid  $[\text{B}(\text{OH})_3]$  and borate ion  $[\text{B}(\text{OH})_4^-]$  varies as a function of pH (Hemming  
331 and Hanson 1992). In addition to the pH dependence of their relative abundances, the boron proxy also relies upon the large  
332 isotopic fractionation between the two boron species (Klochko et al., 2006, Nir et al., 2015). A key assumption of the proxy  
333 is that boron, in the form of borate ion, is the predominant form incorporated into the crystal lattice of calcite via carbonate  
334 ion substitution during the precipitation of calcium carbonate (Hemming and Hanson 1992). The  $\delta^{11}\text{B}$  of the carbonate  
335 ( $\delta^{11}\text{B}_{\text{CaCO}_3}$ ) should then, in theory, reflect the boron isotopic composition of the borate ion ( $\delta^{11}\text{B}_{\text{B}(\text{OH})_4^-}$ ) in the bivalve  
336 calcifying fluid (extrapallial fluid), which in turn reflects pH of the calcifying (extrapallial) fluid.

337 The boron isotopic signature of the shell ( $\delta^{11}\text{B}_{\text{carb}}$ ) was used to calculate pH of the calcifying fluid ( $\text{pH}_{\text{CF}}$ ) using the  
338 following equation (Hemming and Hanson, 1992; Zeebe and Wolf-Gladrow, 2001):

339

$$pH_{cf} = pK_B - \log \left( \frac{\delta^{11}B_{SW} - \delta^{11}B_{carb}}{\delta^{11}B_{SW} - \alpha * \delta^{11}B_{carb} - \varepsilon} \right) \quad \text{eq. 1}$$

341

342 In equation 1,  $pK_B$  is the dissociation constant,  $\delta^{11}B_{sw}$  represents the measured boron isotopic composition of seawater,  
 343  $\delta^{11}B_{carb}$  represents the boron isotopic composition of the shell, and  $\alpha/\varepsilon$  represents the boron isotopic fractionation factor/  
 344 fractionation between boric acid and borate ion (Klochko et al. 2006).¶

345

346 The saturation state of calcite ( $\Omega_{calcite}$ ) and aragonite ( $\Omega_{aragonite}$ ) of the EPF for each species were calculated using  
 347 temperature, salinity, pressure, measured EPF  $Ca^{2+}$ , measured EPF  $Mg^{2+}$ , pH either from microelectrode pH or  
 348  $\delta^{11}B$ -calculated pH, and literature values of DIC (3000 for *A. islandica* from Stemmer et al. 2019, and 4200 for *C. virginica*  
 349 from McNally et al., 2022). The saturation states were calculated using Seacarb with maximum input of  $Mg^{2+}$  allowed by  
 350 the code for samples presenting higher EPF  $Mg^{2+}$  than the limit allowed by the code (Raitzsch et al., 2021). Those saturation  
 351 state values are limited by the fact that no direct measurements of EPF DIC was performed during this study, and a range of  
 352  $Ca^{2+}$  and  $Mg^{2+}$  values were measured in the EPF, resulting in a range of calculated saturation states. The apparent partition  
 353 coefficient calculated as the ratio of E/Ca for the mineral over the E/Ca for seawater. ~~The saturation state of calcite ( $\Omega_{calcite}$ )~~  
 354 ~~and aragonite ( $\Omega_{aragonite}$ ) of the EPF for each species were calculated using temperature, salinity, pressure, measured EPF~~  
 355  ~~$Ca^{2+}$ , measured EPF  $Mg^{2+}$ , pH either from microelectrode pH or  $\delta^{11}B$ -calculated pH, and literature values of DIC (3000~~  
 356 ~~for *A. islandica* from Stemmer et al. 2019, and 4200 for *C. virginica* from McNally et al., 2022). The saturation states were~~  
 357 ~~calculated using Seacarb with maximum input of  $[Mg^{2+}]$  allowed by the code for samples presenting higher EPF  $[Mg^{2+}]$~~   
 358 ~~than the limit allowed by the code (Raitzsch et al., 2021). Those saturation state values are limited by the fact that no direct~~  
 359 ~~measurements of EPF DIC was performed during this study, and a range of  $[Ca^{2+}]$  and  $[Mg^{2+}]$  values were measured in the~~  
 360 ~~EPF, resulting in a range of calculated saturation states as presented in Table 3.~~

## 361 2.8 Statistical analysis

362 All statistical tests were performed and data graphed using GraphPad Prism software version 9 (GraphPad Software  
 363 Inc.; San Diego, CA, USA). Prior to statistical analyses, a Shapiro-Wilks test was run to determine normality and a  
 364 Brown-Forsythe test was used to determine heterogeneity of variance of residuals. Only two comparative t-test data did not  
 365 meet requirements, so a nonparametric Mann-Whitney u test was run in place of a t-test. T-test and Mann-Whitney u tests  
 366 were performed in order to test whether there was a difference between seawater and EPF geochemical parameters and  
 367 between the EPF of both species under ambient conditions. A one-way ANOVA with pH as a four level factor was used to  
 368 test whether pH had a significant effect on our geochemical data. ANOVA and t-test significance was achieved if the p-value  
 369 was less than 0.05. Regression analysis was performed on GraphPad Prism and significance was denoted if the slope of the  
 370 regression was statistically non-zero.

371



### 373 3 Results

#### 374 3.1 ~~Previous~~ Culturing experiment, calcification rates, seawater ~~chemistry~~, and EPF chemistry

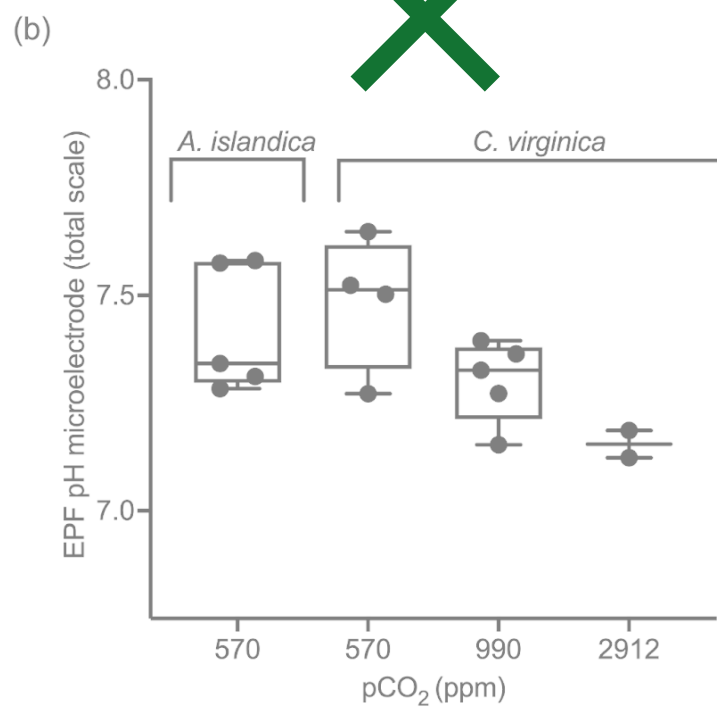
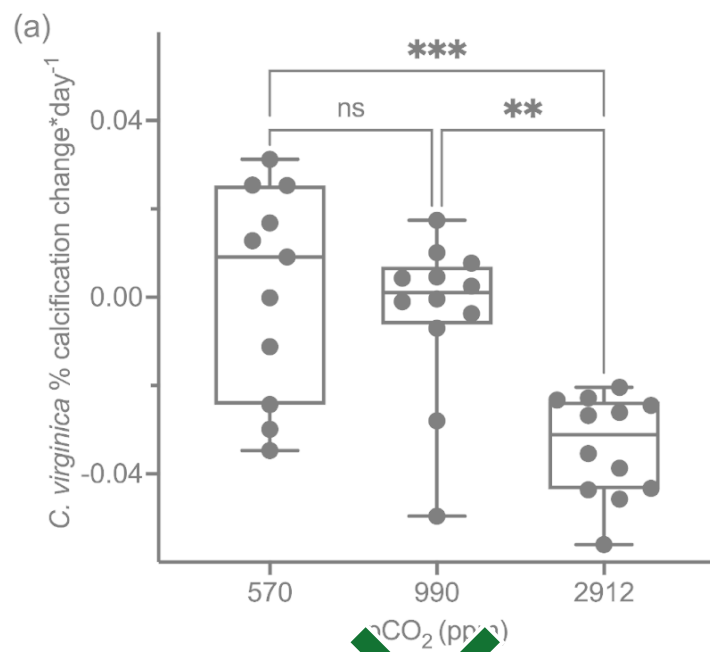
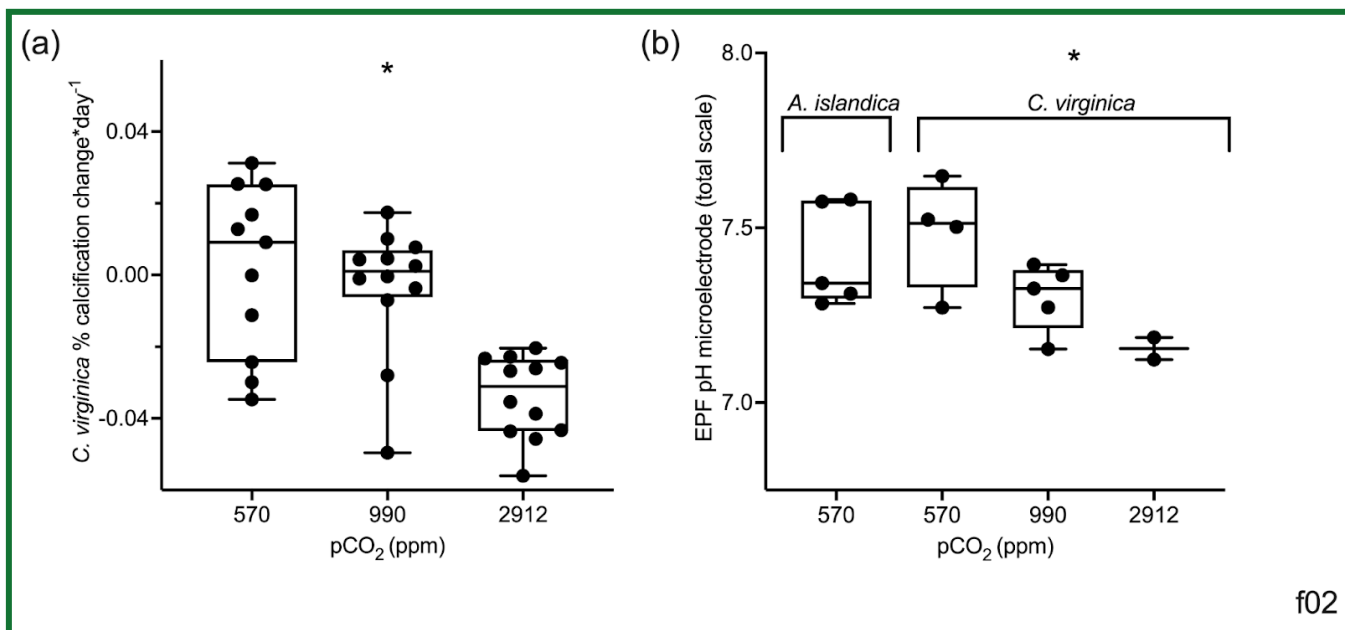


Figure 2. (a) Box plots showing percent calcification change over the experiment for *C. virginica* for each treatment. Stars denote statistically different means and 'ns' signify non significant mean differences in a pairwise t test (at significance  $p < 0.05$ ). (b) Averaged microelectrode EPF pH for *A. islandica* under control conditions and *C. virginica* for OA conditions.

*C. Crassostrea virginica* specimens were previously cultured in experimental tanks with seawater that was continuously bubbled with gas mixtures comprising three  $pCO_2$  levels: (400 ppm, 900 ppm, 2800 ppm; see (Downey-Wall *et al.*, 2020). The tank seawater saturation states of calcite ( $\Omega_{calcite}$ ) was calculated for *C. virginica* under the ocean acidification experiment and not *A. islandica*. As seawater  $pCO_2$  increased, seawater  $\Omega_{calcite}$  decreased. Only the highest  $pCO_2$  treatment produced calcite saturation states seawater values with a  $\Omega_{calcite} < 1$ , which does not favor calcification (Table 1). Similarly to  $\Omega_{calcite}$ , calcification rates were also only measured for the *C. virginica* OA experiment.  $pCO_2$  treatment had a significant effect on *C. virginica* calcification, with the percent change in calcification per day decreasing with increasing  $pCO_2$ . There was also variability in calcification between specimens within each treatment (Fig 2a).



**Figure 2.** (a) Box plots showing percent calcification change over the experiment for *C. virginica* for each treatment. (b) Averaged microelectrode EPF pH for *A. islandica* under control conditions and *C. virginica* for OA treatments. Stars denote a statistically significant ANOVA (at significance  $p < 0.05$ ).

In this study, we present unpublished EPF pH microelectrode data for *A. islandica* cultured at a single control condition (400 ppm  $pCO_2$ ) and we present published EPF microelectrode data for the *C. virginica* acidification experiment of

Downey-Wall et al. (2020). At control seawater conditions the EPF pH of *A. islandica* was 7.41, compared to 7.48 for *C. virginica*. The EPF pH of both species were not statistically different (t-test  $p > 0.05$ ) and the average EPF pH of both species was well under seawater pH (Fig 2b). Measured and calculated seawater parameters from the culture experiments are presented in Table 1. Percent change in calcification per day (Fig 2a), as well as EPF pH as measured by microelectrode (Fig 2B), decreased in *C. virginica* with increasing  $p\text{CO}_2$ . Additionally  $p\text{CO}_2$  treatment also had a significant effect on *C. virginica* EPF pH (ANOVA  $p\text{-value} < 0.05$ ), with microelectrode measure EPF pH decreasing as  $p\text{CO}_2$  increased (Fig 2b). Both species had similar EPF pH (Fig 2b). Downey-Wall et al 2020 reported that *C. virginica* calcification decreased as  $p\text{CO}_2$  increased and that, for each acidification treatment, the mean EPF pH during the experiment was lower than the corresponding seawater pH. Additionally, they Downey-Wall et al. (2020) also report that using a linear model,  $p\text{CO}_2$  treatment had a significant effect on EPF pH (linear model,  $p < 0.05$ ) and that at the highest  $p\text{CO}_2$  treatment, EPF pH was significantly lower than seawater pH (Table 1, Fig 2, post hoc  $p\text{-value} < 0.05$  see Downey-Wall et al., 2020). We report that the change in pH ( $\Delta\text{pH}$ ) for both species as the *C. virginica* average  $\Delta\text{pH}$  (seawater pH - EPF pH). The  $\Delta\text{pH}$  for *A. islandica* was 0.52 and was similar to the control condition  $\Delta\text{pH}$  for *C. virginica* which was 0.53 (Table 1). Under OA treatments,  $\Delta\text{pH}$  for *C. virginica* decreased with decreasing seawater pH. The  $\Delta\text{pH}$  for the control treatment was 0.53, the moderate OA treatment was 0.46, and the high OA treatment was 0.08.

	Control <i>A. islandica</i>	Control <i>C. virginica</i>	Moderate OA <i>C. virginica</i>	High OA <i>C. virginica</i>
	EPF geochemistry			
EPF pH	7.41 ± 0.14	7.48 ± 0.15	7.29 ± 0.10	7.21 ± 0.10
$\Delta\text{pH}_{\text{SW-EPF}}$	0.52	0.53	0.46	0.08
Mg/Ca	4.25 ± 0.67	4.55 ± 0.50	5.73 ± 0.34	5.58 ± 0.46
$\delta^{26}\text{Mg}$	-0.69 ± 0.1	-0.88 ± 0.06	-0.87 ± 0.07	-0.9 ± 0.1
B/Ca	31.17 ± 4.87	33.66 ± 2.81	42.22 ± 3.33	43.26 ± 2.82
$\delta^{11}\text{B}$	39.5 ± 0.4	39.3 ± 1.0	38.9 ± 0.4	n/d
	Shell geochemistry			
Mg/Ca	0.8 ± 0.2	13.8 ± 1.7	13.4 ± 2.3	12.3 ± 1.5
$\delta^{26}\text{Mg}$	n/d	-3.2 ± 0.1	-3.1 ± 0.1	-3.0 ± 0.2

B/Ca	57 ± 17	114 ± 22	125 ± 11	124 ± 9
δ <sup>11</sup> B	15.2 ± 0.4	18.3 ± 0.5	16.9 ± 0.5	16.8 ± 0.3

Table 2. Measured extrapallial fluid (EPF) carbonate chemistry parameters (pH, DIC, TA, Ω, δ<sup>11</sup>B-calculated EPF pH, and ΔpH) for both *C. virginica* and *A. islandica* under control conditions and *C. virginica* for OA conditions. Extrapallial fluid and shell geochemical parameters (Mg/Ca, δ<sup>26</sup>Mg, B/Ca, δ<sup>11</sup>B) for both *C. virginica* and *A. islandica* under control conditions and *C. virginica* for OA conditions. Parameters that were unable to be not measured due to insufficient sample size or unable to be calculated are marked with ‘n/d.’

	Control <i>A. islandica</i>	Control <i>C. virginica</i>	Moderate OA <i>C. virginica</i>	High OA <i>C. virginica</i>
EPF geochemistry				
EPF pH	7.41 ± 0.14	7.48 ± 0.15	7.29 ± 0.10	7.21 ± 0.10
ΔpH <sub>SW-EPF</sub>	0.52	0.53	0.46	0.08
Mg/Ca	4.25 ± 0.67	4.55 ± 0.50	5.73 ± 0.34	5.58 ± 0.46
δ <sup>26</sup> Mg	-0.69 ± 0.1	-0.88 ± 0.06	-0.87 ± 0.07	-0.9 ± 0.1
B/Ca	31.17 ± 4.87	33.66 ± 2.81	42.22 ± 3.33	43.26 ± 2.82
δ <sup>11</sup> B	39.5 ± 0.4	39.3 ± 1.0	38.9 ± 0.4	n/d
Shell geochemistry				
Mg/Ca	0.8 ± 0.2	13.8 ± 1.7	13.4 ± 2.3	12.3 ± 1.5
δ <sup>26</sup> Mg	n/d	-3.2 ± 0.1	-3.1 ± 0.1	-3.0 ± 0.2
B/Ca	57 ± 17	114 ± 22	125 ± 11	124 ± 9
δ <sup>11</sup> B	15.2 ± 0.4	18.3 ± 0.5	16.9 ± 0.5	16.8 ± 0.3

420 **Table 2.** Measured extrapallial fluid (EPF) carbonate chemistry parameters (pH, DIC, TA,  $\Omega$ ,  $\delta^{11}\text{B}$ -calculated EPF pH, and  
421  $\Delta\text{pH}$ ) for both *C. virginica* and *A. islandica* under control conditions and *C. virginica* for OA conditions. Extrapallial fluid  
422 and shell geochemical parameters (Mg/Ca,  $\delta^{26}\text{Mg}$ , B/Ca,  $\delta^{11}\text{B}$ ) for both *C. virginica* and *A. islandica* under control conditions  
423 and *C. virginica* for OA conditions. Parameters that were unable to be not measured due to insufficient sample size or unable  
424 to be calculated are marked with 'n/d.'

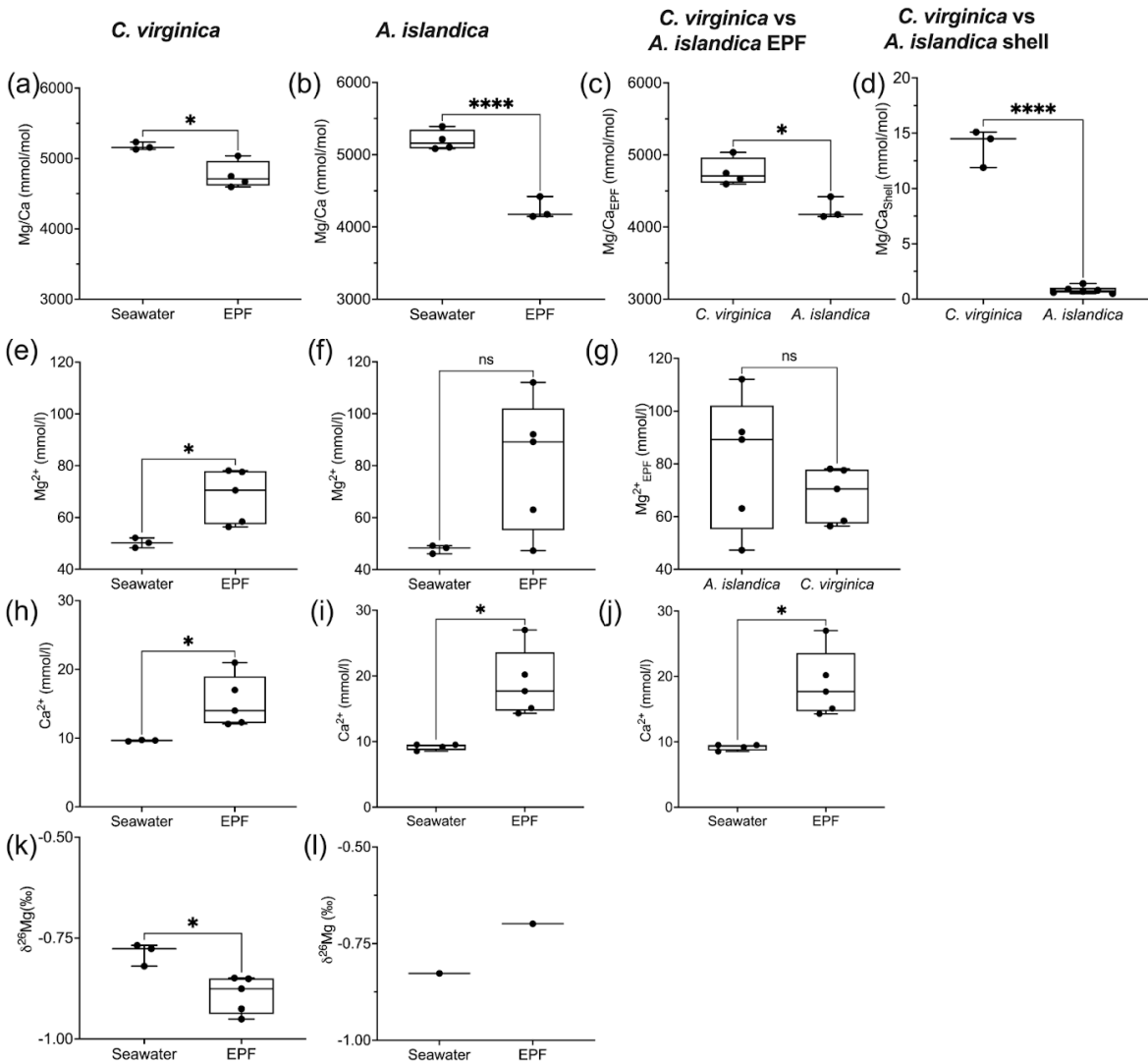
425

### 426 **3.2 Comparison of *A. islandica* and *C. virginica* geochemistry of seawater, EPF, and bivalve shell**

427       There was a significant decrease in EPF Mg/Ca compared to seawater Mg/Ca for both *A. islandica* and *C. virginica*  
428 (t-test,  $n=2$ ,  $p\text{-value}<0.05$ ; Fig 3a-b). The Mg/Ca of *C. virginica* EPF was  $4.55 \pm 0.50$  mol/mol and significantly higher than  
429 *A. islandica* EPF which was  $4.25 \pm 0.67$  mol/mol (Fig 3d; Table 2). For both species, the low EPF Mg/Ca versus seawater  
430 Mg/Ca was driven by higher  $\text{Ca}^{2+}$  concentrations in the EPF relative to seawater (Fig 3h-i). Considering the elemental  
431 concentrations alone, instead of as a ratio, there was no significant difference in EPF  $\text{Mg}^{2+}$  or  $\text{Ca}^{2+}$  concentrations between  
432 species (Fig 3g and 3j). Shell Mg/Ca for the calcitic *C. virginica* was  $13.8 \pm 1.7$  mmol/mol and significantly higher than the  
433 aragonitic *A. islandica* shell which was  $0.8 \pm 0.02$  mmol/mol, in line with shell polymorph mineralogy. The apparent partition  
434 coefficient ( $K_{\text{Mg}}$ ) between the seawater and the shell was 0.003 in *C. virginica* and 0.002 in *A. islandica* (Table 3).  $K_{\text{Mg}}$   
435 between EPF and shell was 0.003 in *C. virginica* and 0.002 in *A. islandica*.  $K_{\text{Mg}}$  between seawater and the EPF is 0.9 for *C.*  
436 *virginica* and 0.8 for *A. islandica* (Table 3). *C. virginica* seawater and EPF  $\delta^{26}\text{Mg}$  were  $-0.77 \pm 0.01$  ‰ and  $-0.88 \pm 0.06$  ‰,  
437 respectively and displayed a significant decrease in EPF  $\delta^{26}\text{Mg}$  compared to seawater for *C. virginica* (t-test,  $n_1=3$   $n_2=5$ ,  
438  $p\text{-value}<0.05$ ; Fig 3k-l). For *A. islandica*, seawater and EPF  $\delta^{26}\text{Mg}$  were  $-0.82 \pm 0.06$  ‰ and  $-0.69 \pm 0.01$  ‰, respectively,  
439 but no statistical analysis could be done between the two reservoirs owing to the small sample size (Table 1 and 2). The  
440 average shell  $\delta^{26}\text{Mg}$  for *C. virginica* was  $-3.2 \pm 0.1$ ‰, but *A. islandica* shell  $\delta^{26}\text{Mg}$  could not be analyzed because of low  
441 shell  $[\text{Mg}^{2+}]$  content and limited sample material.

442       There was a significant decrease in EPF Mg/Ca compared to seawater Mg/Ca for both *A. islandica* and *C. virginica*  
443 (t-test,  $n=2$ ,  $p\text{-value}<0.05$ ; Fig 3a-b). The Mg/Ca of *C. virginica* EPF was  $4.55 \pm 0.50$  mol/mol and significantly higher than  
444 *A. islandica* EPF which was  $4.25 \pm 0.67$  mol/mol (Fig 3d; Table 2). For both species, the low EPF Mg/Ca versus seawater  
445 Mg/Ca was driven by higher  $\text{Ca}^{2+}$  concentrations in the EPF relative to seawater (Fig 3h-i). Considering the elemental  
446 concentrations alone, instead of as a ratio, there was no significant difference in EPF  $\text{Mg}^{2+}$  or  $\text{Ca}^{2+}$  concentrations between  
447 species (Fig 3g and 3j). Shell Mg/Ca for the calcitic *C. virginica* was  $13.8 \pm 1.7$  mmol/mol and significantly higher than the  
448 aragonitic *A. islandica* shell which was  $0.8 \pm 0.02$  mmol/mol, in line with shell polymorph mineralogy. The apparent partition  
449 coefficient ( $K_{\text{Mg}}$ ) between the seawater and the shell was 0.003 in *C. virginica* and 0.002 in *A. islandica* (Table 3).  $K_{\text{Mg}}$   
450 between EPF and shell was 0.003 in *C. virginica* and 0.002 in *A. islandica*.  $K_{\text{Mg}}$  between seawater and the EPF is 0.9 for *C.*  
451 *virginica* and 0.8 for *A. islandica* (Table 2). *C. virginica* seawater and EPF  $\delta^{26}\text{Mg}$  were  $-0.77 \pm 0.01$  ‰ and  $-0.88 \pm 0.06$

452 %, respectively and displayed a significant decrease in EPF  $\delta^{26}\text{Mg}$  compared to seawater for *C. virginica* (t-test,  $n_1=3$   $n_2=5$ ,  
 453 p-value < 0.05; Table 1, Fig 3k l). For *A. islandica*, seawater and EPF  $\delta^{26}\text{Mg}$  were  $-0.82 \pm 0.06$  ‰ and  $-0.69 \pm 0.01$  ‰,  
 454 respectively, but no statistical analysis could be done between the two reservoirs owing to the small sample size (Table 21).  
 455 The average shell  $\delta^{26}\text{Mg}$  for *C. virginica* was  $-3.2 \pm 0.1$  ‰, but *A. islandica* shell  $\delta^{26}\text{Mg}$  could not be analyzed because of  
 456 low shell  $[\text{Mg}^{2+}]$  content and limited sample material.



457  
 458 **Figure 3.** Box plots of Mg/Ca comparing seawater and extrapallial fluid for (a) *C. virginica* and (b) *A. islandica*,  
 459 (c) comparing EPF Mg/Ca between species, and (d) shell Mg/Ca between species. Box plots of  $[\text{Mg}^{2+}]$  comparing seawater  
 460 and extrapallial fluid for (e) *C. virginica* and (f) *A. islandica*, (g) comparing EPF  $[\text{Mg}^{2+}]$  between species. Box plots of  $[\text{Ca}]$   
 461 comparing seawater and extrapallial fluid for (h) *C. virginica* and (i) *A. islandica*, (j) comparing EPF  $[\text{Ca}]$  between species.



Box plots of  $\delta^{26}\text{Mg}$  comparing seawater and extrapallial fluid for (k) *C. virginica* and (l) *A. islandica*. Stars denote statistically different means and ‘ns’ signify non significant mean differences in a pairwise t-test or Mann-Whitney u test (at significance  $p < 0.05$ ). No comparison was tested on (l) due to limited sample size.

Box plots of Mg/Ca comparing seawater and extrapallial fluid for (a) *C. virginica* and (b) *A. islandica*, (c) comparing EPF Mg/Ca between species, and (d) shell Mg/Ca between species. Box plots of  $[\text{Mg}^{2+}]$  comparing seawater and extrapallial fluid for (e) *C. virginica* and (f) *A. islandica*, (g) comparing EPF  $[\text{Mg}^{2+}]$  between species. Box plots of  $[\text{Ca}]$  comparing seawater and extrapallial fluid for (h) *C. virginica* and (i) *A. islandica*, (j) comparing EPF  $[\text{Ca}]$  between species. Box plots of  $\delta^{26}\text{Mg}$  comparing seawater and extrapallial fluid for (k) *C. virginica* and (l) *A. islandica*. Stars denote statistically different means and ‘ns’ signify non significant mean differences in a pairwise t-test (at significance  $p < 0.05$ ). No comparison was tested on (l) due to limited sample size.

472

473

474

475

<i>A. islandica</i>		<i>C. virginica</i>			
		$p\text{CO}_2$	400	900	28000
$K_{\text{Mg}}$	0.0002		0.003	0.002	0.002
$K_{\text{B}}$	0.001		0.003	0.003	0.003

**Table 3.** Partition coefficients between seawater and the mineral for Mg/Ca and B/Ca.

477

478

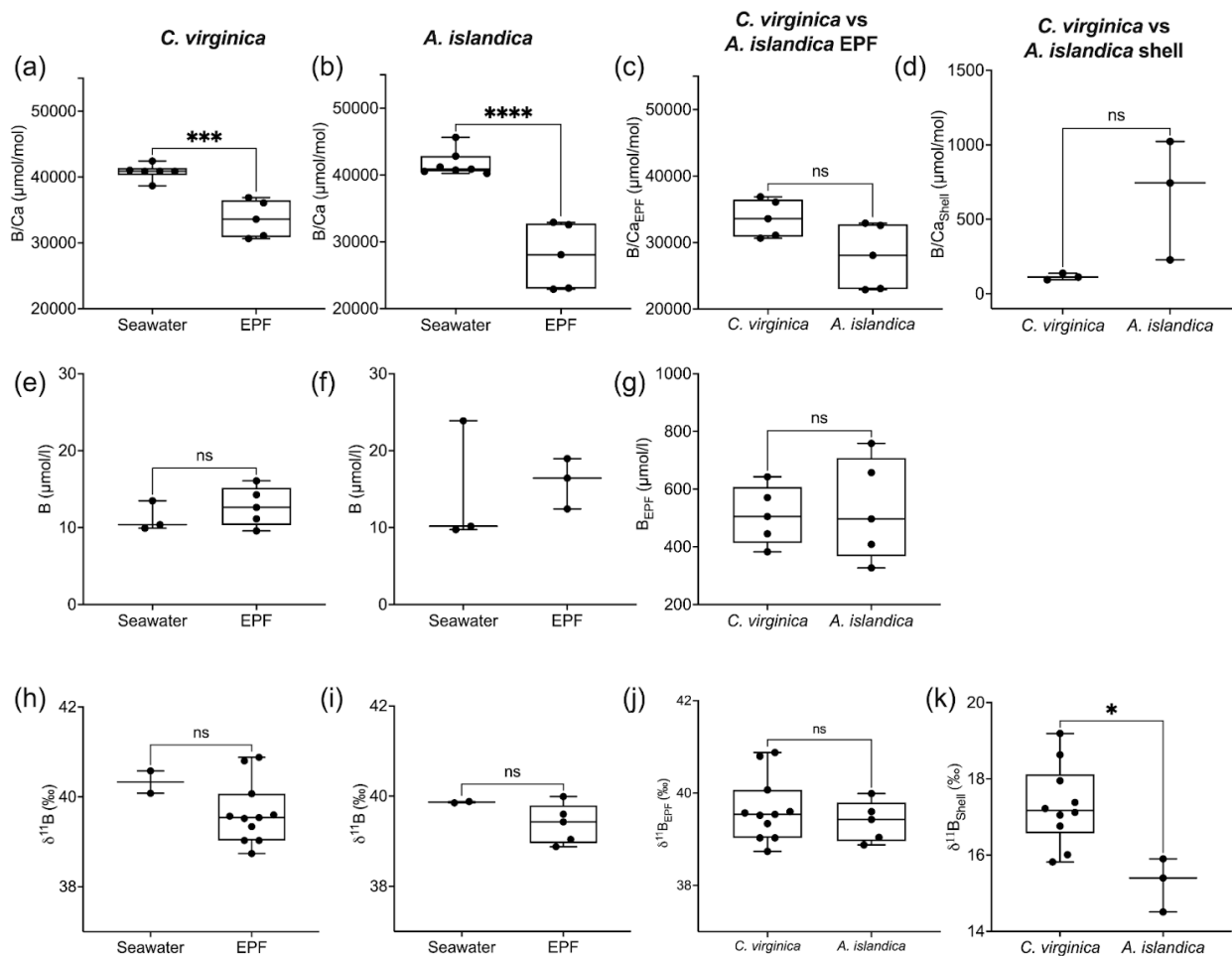
	<i>A. islandica</i>		<i>C. virginica</i>		
		$p\text{CO}_2$	400	900	28000
$K_{\text{Mg}}$	0.0002		0.003	0.002	0.002
$K_{\text{B}}$	0.001		0.003	0.003	0.003

**Table 2.** Partition coefficients between EPF and seawater, seawater and the mineral, and EPF and the mineral for Mg/Ca and B/Ca.

*A. islandica* EPF B/Ca was  $27.91 \pm 4.87$  mmol/mol and was significantly lower than seawater B/Ca which was  $41.75 \pm 1.52$  mmol/mol (t-test,  $n_1=7$   $n_2=5$ ,  $p\text{-value}<0.05$ , Fig 4a). *C. virginica* EPF B/Ca was  $41.66 \pm 1.07$  mmol/mol and was significantly lower than seawater B/Ca which was  $33.66 \pm 2.81$  mmol/mol (t-test,  $n_1=6$   $n_2=5$ ,  $p\text{-value}<0.05$  Fig 4b) The boron concentration was not significantly different between seawater and EPF for both *C. virginica* and *A. islandica* (Fig

485 4e-f). There was no significant difference in shell or EPF B/Ca between *C. virginica* and *A. islandica* (Fig 4c-d). The  
486 apparent partition coefficient ( $K_B$ ) between the seawater and the shell was 0.003 in *C. virginica* and 0.001 in *A. islandica*.  $K_B$   
487 between EPF and shell was 0.003 in *C. virginica* and 0.002 in *A. islandica*.  $K_B$  between seawater and the EPF is 0.8 in *C.*  
488 *virginica* and 0.7 for *A. islandica* (Table 3). There was no significant difference in  $\delta^{11}\text{B}$  between seawater and EPF for both  
489 species in the control condition (Fig 4h-l). There was also no significant difference in EPF  $\delta^{11}\text{B}$  between species(Fig 4j);  
490 however, there was a significant difference in shell  $\delta^{11}\text{B}$  between *C. virginica* and *A. islandica* (t-test,  $n_1=10$   $n_2=3$ ,  
491  $p\text{-value}<0.05$ , Fig 4k). Under control conditions, shell  $\delta^{11}\text{B}$  was measured to be  $15.26 \pm 0.41\text{‰}$  (2 SD,  $n=3$ ) for *C. virginica*  
492 and  $18.34 \pm 0.59 \text{‰}$  (2 SD,  $n=3$ ) for *A. islandica*.

493 ~~A. islandica EPF B/Ca was  $27.91 \pm 4.87$  mmol/mol and was significantly lower than seawater B/Ca which was~~  
494  ~~$41.75 \pm 1.52$  mmol/mol (t test,  $n_1=7$   $n_2=5$ ,  $p\text{-value}<0.05$ , Fig 4a). *C. virginica* EPF B/Ca was  $41.66 \pm 1.07$  mmol/mol and~~  
495 ~~was significantly lower than seawater B/Ca which was  $33.66 \pm 2.81$  mmol/mol (t test,  $n_1=6$   $n_2=5$ ,  $p\text{-value}<0.05$  Fig 4b) The~~  
496 ~~boron concentration was not significantly different between seawater and EPF for both *C. virginica* and *A. islandica* (Fig~~  
497 ~~4e-f). There was no significant difference in shell or EPF B/Ca between *C. virginica* and *A. islandica* (Fig 4e-d). The~~  
498 ~~apparent partition coefficient ( $K_B$ ) between the seawater and the shell was 0.003 in *C. virginica* and 0.001 in *A. islandica*.~~  
499  ~~$K_B$  between EPF and shell was 0.003 in *C. virginica* and 0.002 in *A. islandica*.  $K_B$  between seawater and the EPF is 0.8 in~~  
500 ~~*C. virginica* and 0.7 for *A. islandica* (Table 3). There was no significant difference in  $\delta^{11}\text{B}$  between seawater and EPF for~~  
501 ~~both species in the control condition (Fig 4h-l). There was also no significant difference in EPF  $\delta^{11}\text{B}$  between species(Fig~~  
502 ~~4j); however, there was a significant difference in shell  $\delta^{11}\text{B}$  between *C. virginica* and *A. islandica* (t-test,  $n_1=10$   $n_2=3$ ,~~  
503  ~~$p\text{-value}<0.05$ , Fig 4k). Under control conditions, shell  $\delta^{11}\text{B}$  was measured to be  $15.26 \pm 0.41\text{‰}$  (2 SD,  $n=3$ ) for *C. virginica*~~  
504 ~~and  $18.34 \pm 0.59 \text{‰}$  (2 SD,  $n=3$ ) for *A. islandica*.~~



f 04

505

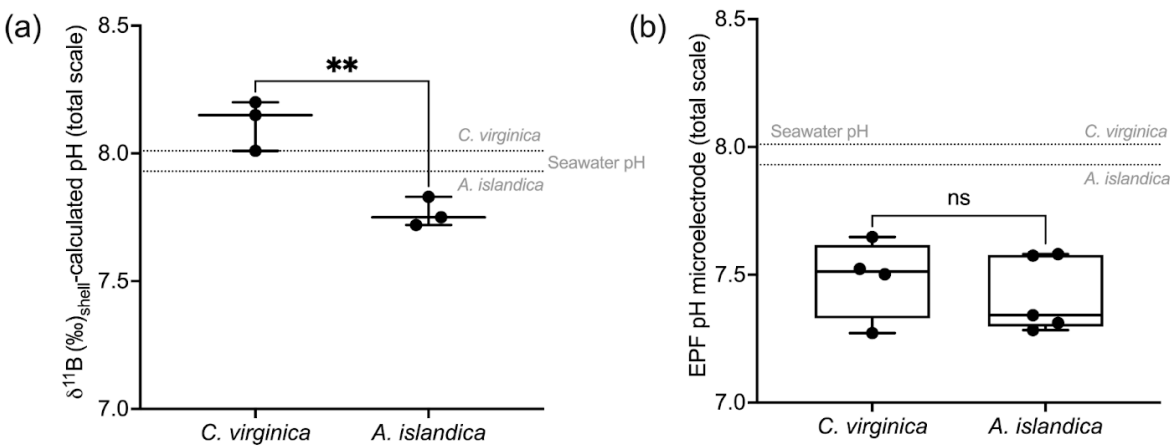
506 **Figure 4.** Box plots of B/Ca comparing seawater and extrapallial fluid for (a) *C. virginica* and (b) *A. islandica*, (c)  
 507 comparing EPF B/Ca between species, and (d) shell B/Ca between species. Box plots of [B] comparing seawater and  
 508 extrapallial fluid for (e) *C. virginica* and (f) *A. islandica*, (g) comparing EPF [B] between species. Box plots of δ¹¹B  
 509 comparing seawater and extrapallial fluid for (h) *C. virginica* and (i) *A. islandica*, comparing EPF δ¹¹B between species, and  
 510 (d) shell δ¹¹B between species. Stars denote statistically different means and 'ns' signify non significant mean differences in  
 511 a pairwise t-test or Mann-Whitney u test (at significance  $p < 0.05$ ).

512



513 ~~Figure 46.~~ Box plots of B/Ca comparing seawater and extrapallial fluid for (a) *C. virginica* and (b) *A. islandica*, (c)  
 514 ~~comparing EPF B/Ca between species, and (d) shell B/Ca between species. Box plots of [B] comparing seawater and~~  
 515 ~~extrapallial fluid for (e) *C. virginica* and (f) *A. islandica*, (g) comparing EPF [B] between species. Box plots of δ¹¹B~~

516 comparing seawater and extrapallial fluid for (h) *C. virginica* and (i) *A. islandica*, comparing EPF  $\delta^{11}\text{B}$  between species, and  
 517 (d) shell  $\delta^{11}\text{B}$  between species. Stars denote statistically different means and ‘ns’ signify non significant mean differences in  
 518 a pairwise t-test (at significance  $p < 0.05$ ).



519  
 520  
 521 **Figure 59.** (a) Box plot of  $\delta^{11}\text{B}$ -calculated pH for *C. virginica* and *A. islandica*. (b) Box plot of measured microelectrode pH  
 522 for *C. virginica* and *A. islandica*. The grey line shows seawater pH for *C. virginica* and *A. islandica*. Stars denote statistically  
 523 different means and ‘ns’ signify non significant mean differences in a pairwise t-test (at significance  $p < 0.05$ ).

524 **Figure 59.** (a) Box plot of  $\delta^{11}\text{B}$ -calculated pH for *C. virginica* and *A. islandica*. (b) Box plot of measured microelectrode pH  
 525 for *C. virginica* and *A. islandica*. The grey line shows seawater pH for *C. virginica* and *A. islandica*. Stars denote statistically  
 526 different means and ‘ns’ signify non significant mean differences in a pairwise t-test (at significance  $p < 0.05$ ).

527 The control condition  $\delta^{11}\text{B}$ -calculated EPF pH for *C. virginica* was  $8.12 \pm 0.08$  ‰ (2 SD,  $n=3$ ) and for *A. islandica* was  $7.93$   
 528  $\pm 0.09$  ‰ (2 SD,  $n=3$ ), which yielded a statistically significant difference between the two species (t-test,  $n_1=3$   $n_2=3$ ,  
 529  $p\text{-value}<0.05$ , Fig 59a). For *C. virginica*, the  $\delta^{11}\text{B}$ -calculated EPF was 0.1 pH units higher than the seawater pH and 0.6  
 530 lower than measured EPF pH. Conversely, the *A. islandica*  $\delta^{11}\text{B}$ -calculated EPF was 0.1 pH units lower than the seawater  
 531 pH and 0.3 higher than the measured EPF pH (Fig 59).

532

Control	Control	Moderate OA	High OA

	<i>A. islandica</i> ( $\Omega$ aragonite)	<i>C. virginica</i> ( $\Omega$ calcite)	<i>C. virginica</i> ( $\Omega$ calcite)	<i>C. virginica</i> ( $\Omega$ calcite)
$\Omega$ using EPF pH (range)	1.7 (1.0-3.8)	3.7 (1.3-11.4)	1.1 (0.5-2)	0.9 (0.5-1.2)
$\Omega$ using $\delta^{11}\text{B}$ -calculated pH (range)	3.8 (2.9-6.7)	15.4 (6.7-37)	6.1 (3-11.7)	6.5 (3.4-9.7)

533

534 **Table 4.** Table of calculated saturation state ( $\Omega$ ) with respect to calcite (*C. virginica*) or aragonite (*A. islandica*) for the  
535 average EPF pH value based on microelectrode measurements or  $\delta^{11}\text{B}$ -calculated EPF pH.

536 ¶¶

	Control ¶¶	Control ¶¶	Moderate OA ¶¶	High OA ¶¶
	<i>A. islandica</i> ( $\Omega$ aragonite) ¶	<i>C. virginica</i> ( $\Omega$ calcite) ¶¶	<i>C. virginica</i> ( $\Omega$ calcite) ¶¶	<i>C. virginica</i> ( $\Omega$ calcite) ¶¶
$\Omega$ using EPF pH ¶¶	1.7 (1.0-3.8) ¶	3.7 (1.3-11.4) ¶¶	1.1 (0.5-2) ¶¶	0.9 (0.5-1.2) ¶¶
$\Omega$ using $\delta^{11}\text{B}$ -calculated pH (range) ¶¶	3.8 (2.9-6.7) ¶	15.4 (6.7-37) ¶¶	6.1 (3-11.7) ¶¶	6.5 (3.4-9.7) ¶¶

537 ¶¶

538 ¶¶

539 ¶¶

540 ~~Table 43.~~ Table of calculated saturation state ( $\Omega$ ) with respect to calcite (*C. virginica*) or aragonite (*A. islandica*) for the  
541 ~~average EPF pH value based on microelectrode measurements or  $\delta^{11}\text{B}$ -calculated EPF pH.~~

542 In Table 4, the EPF aragonite saturation state ( $\Omega$ aragonite) for *A. islandica* and EPF calcite saturation state  
543 ( $\Omega$ calcite) for *C. virginica* were calculated using the averaged measured EPF pH and averaged  $\delta^{11}\text{B}$ -calculated EPF pH,  
544 averaged measured  $\text{Mg}^{2+}$  and  $\text{Ca}^{2+}$ , and literature values of DIC (3000  $\mu\text{mol/L}$  for *A. islandica* taken from Stemmer et al.  
545 (2019) and 4200  $\mu\text{mol/L}$  for *C. virginica* from McNally et al. (2022). Under control conditions, the *A. islandica*  $\Omega$ aragonite  
546 and *C. virginica*  $\Omega$ calcite that was calculated using  $\delta^{11}\text{B}$ -calculated EPF pH and measured EPF pH (Table 4). Under the  
547 ocean acidification experiment, EPF  $\Omega$ calcite decreased with decreasing seawater pH when using either EPF pH or  
548  $\delta^{11}\text{B}$ -calculated EPF pH to calculate EPF  $\Omega$ calcite. There were large differences in *A. islandica*  $\Omega$ aragonite and *C. virginica*

549  $\Omega_{\text{calcite}}$  when using either EPF pH ( $\Omega_{\text{aragonite}}=1.7$  and  $\Omega_{\text{calcite}}=3.7$ ) or the  $\delta^{11}\text{B}$ -calculated pH ( $\Omega_{\text{aragonite}}=3.8$  and  
550  $\Omega_{\text{calcite}}=15.4$ ).

551

552 3.34 *C. virginica* ocean acidification experiment geochemistry ¶

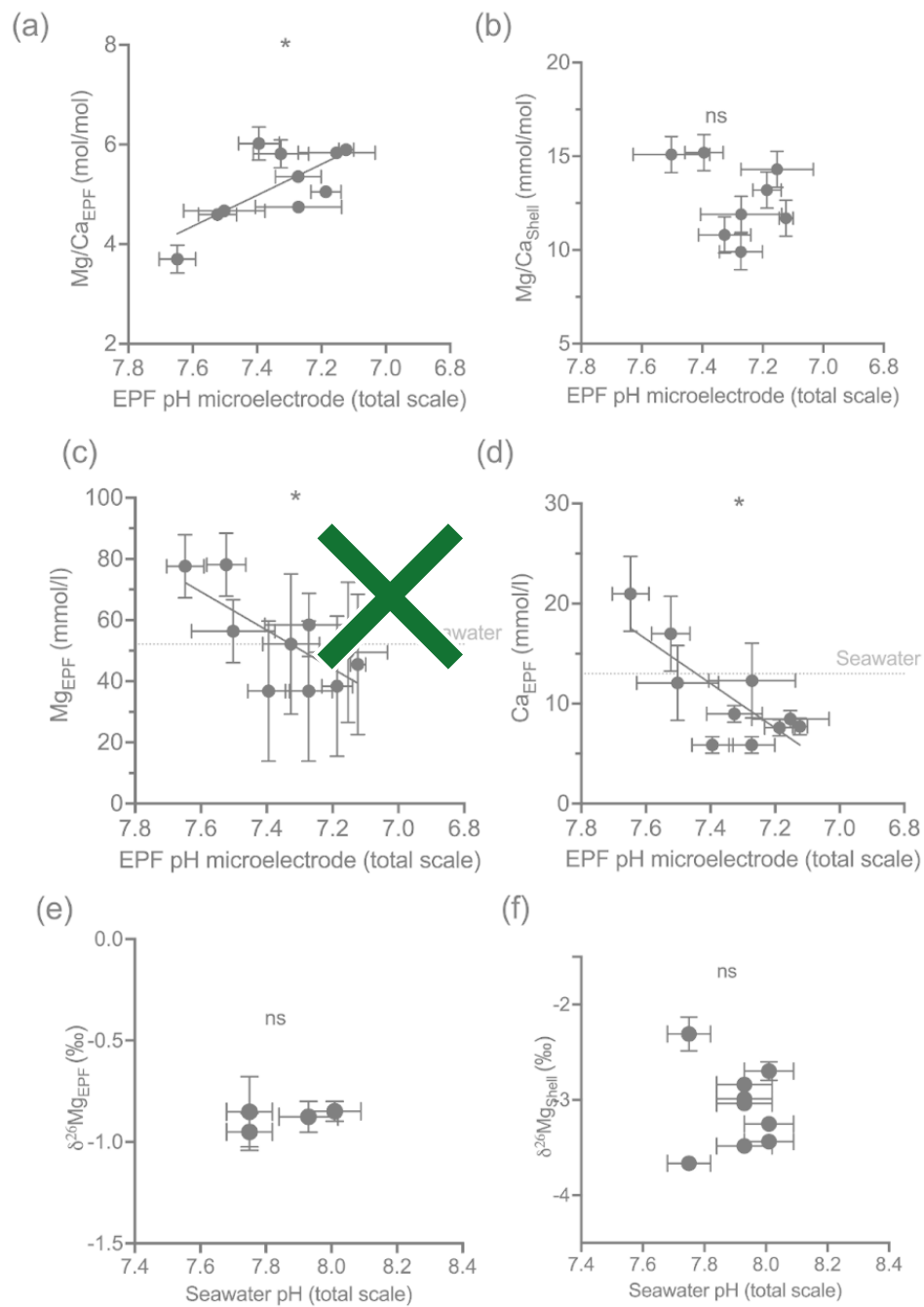
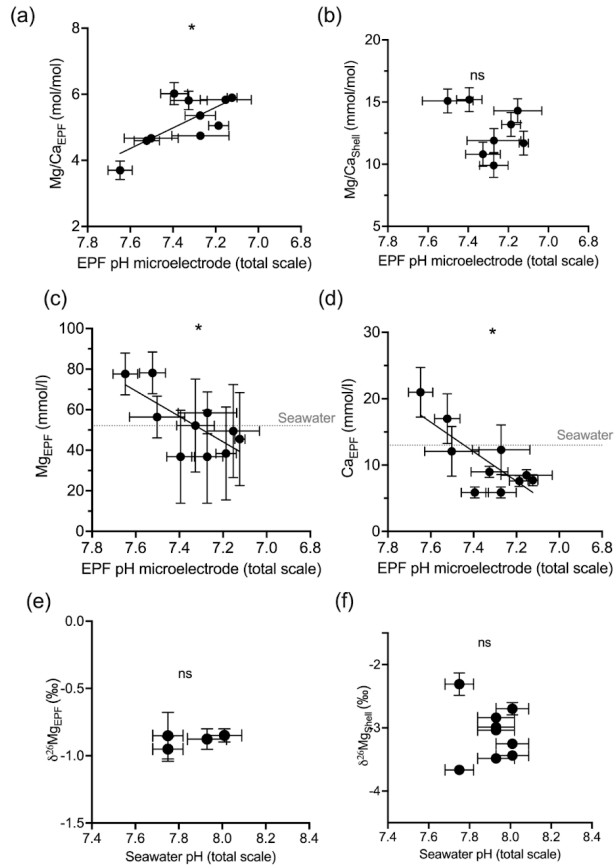




Figure 6. Scatter plots showing *C. virginica* individual specimen (a) EPF Mg/Ca and (b) shell Mg/Ca across corresponding microelectrode pH. Additionally, scatter plots (c) EPF  $Mg^{2+}$ , (d) EPF  $Ca^{2+}$ , (e) EPF  $\delta^{26}Mg$ , and (f) shell  $\delta^{26}Mg$  across microelectrode EPF pH. Stars denote statistically significantly nonzero regression slopes and 'ns' signify non significant regressions (at significance  $p < 0.05$ ). Dotted gray lines on (c) and (d) show the average  $Mg^{2+}$  and  $Ca^{2+}$  seawater concentration, respectively.

In the *C. virginica* acidification experiment, EPF but not shell Mg/Ca was found to increase as EPF pH decreased (regression,  $n=10$ ,  $p\text{-value}<0.05$ ; Fig 6a-b). OA treatment had a significant effect on shell Mg/Ca (ANOVA,  $n=10$ ,  $p\text{-value}<0.05$ , Fig 6a-b). The concentration of both  $Ca^{2+}$  and  $Mg^{2+}$  in the EPF decreased with decreasing EPF pH (regression,  $n=10$ ,  $p\text{-value}< 0.05$ ; Fig 6c-d). However, when binning by seawater pH treatments, only the  $Ca^{2+}$  and  $Mg^{2+}$  of the ambient condition was significantly elevated compared to the moderate and high ocean acidification treatments (Tukey HSD,  $n1=4$   $n2=3$ ,  $p<0.05$ , Fig 6c-d). The EPF and shell  $\delta^{26}Mg$  did not change as a function of EPF or seawater pH (Fig 6e-f and 5e-f).

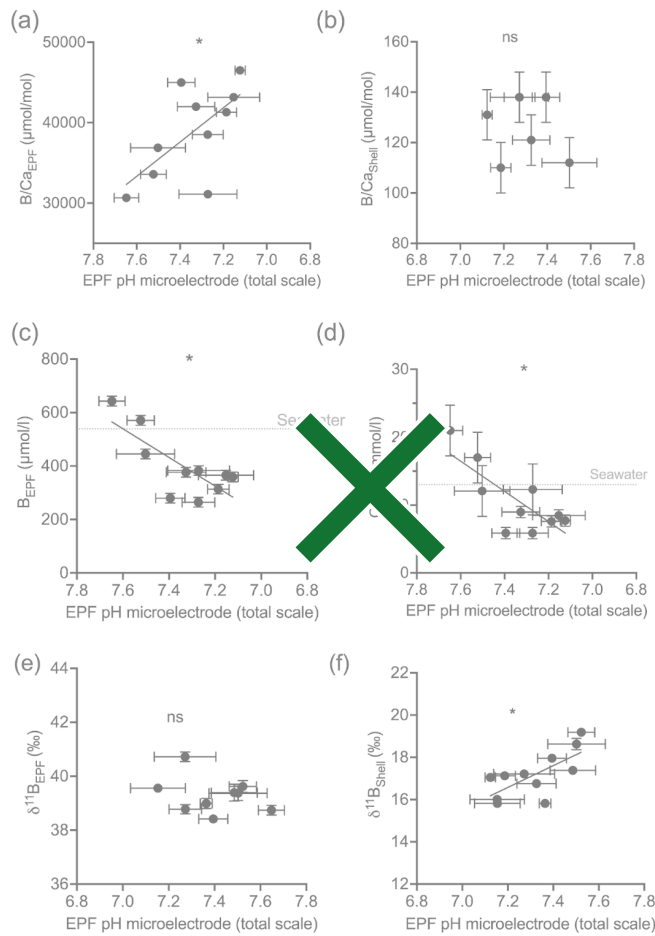


f 06

566

567 **Figure 6.** Scatter plots showing *C. virginica* individual specimen (a) EPF Mg/Ca and (b) shell Mg/Ca across corresponding  
 568 microelectrode pH. Additionally, scatter plots (c) EPF Mg<sup>2+</sup>, (d) EPF Ca<sup>2+</sup>, (e) EPF  $\delta^{26}\text{Mg}$ , and (f) shell  $\delta^{26}\text{Mg}$  across  
 569 microelectrode EPF pH. Dotted gray lines on (c) and (d) show the average Mg<sup>2+</sup> and Ca<sup>2+</sup> seawater concentration,  
 570 respectively. Stars denote statistically significantly nonzero regression slopes and 'ns' signify non significant regressions (at  
 571 significance  $p < 0.05$ ).

572



573

574 Figure 7. Scatter plots showing *C. virginica* individual specimen (a) EPF B/Ca and (b) shell B/Ca across corresponding  
 575 microelectrode EPF pH. Additionally, scatter plots of (c) EPF B, (d) EPF Ca<sup>2+</sup>, (e) EPF δ<sup>11</sup>B, and (f) shell δ<sup>11</sup>B across  
 576 microelectrode EPF pH. Stars denote statistically significantly nonzero regression slopes and 'ns' signify non significant  
 577 regressions (at significance  $p < 0.05$ ). Dotted gray lines on (c) and (d) show the average B and Ca<sup>2+</sup> seawater concentration,  
 578 respectively.

579 Under OA conditions, EPF B/Ca but not shell B/Ca was found to increase as seawater pH decreased (ANOVA  $p$ -value $<0.05$ ,  
 580 compare Fig 7a-b). The EPF but not shell B/Ca was found to increase as EPF pH decreased (regression  $p$ -value $< 0.05$ , Fig  
 581 78a-b). The boron concentration of the EPF, but not the shell, significantly decreased with decreasing EPF pH (regression  
 582  $p$ -value $< 0.05$ , Fig 78c). The EPF B concentration increased with increasing seawater pH (ANOVA  $p$ -value $< 0.05$ , Fig 78c);  
 583 however, shell boron concentrations did not significantly change with seawater pH. Due to small EPF sample volume, EPF  
 584 for the oysters in the lowest seawater pH treatment was not measured for δ<sup>11</sup>B. There was a significant difference in mean

EPF  $\delta^{11}\text{B}$  between the control pH treatment which was 39.39 ‰ and moderate pH treatment which was 38.92 ‰ (t-test,  $n_1=11$   $n_2=7$ ,  $p\text{-value}<0.05$ , Fig 7e-f). The difference between seawater  $\delta^{11}\text{B}$  and EPF  $\delta^{11}\text{B}$  was 0.91 ‰ for the control treatment and decreased to 0.47 ‰ for the moderate pH treatment. Shell  $\delta^{11}\text{B}$ , but not EPF  $\delta^{11}\text{B}$ , significantly decreased with decreasing EPF pH (regression  $p\text{-value}<0.05$ , Fig 7f).

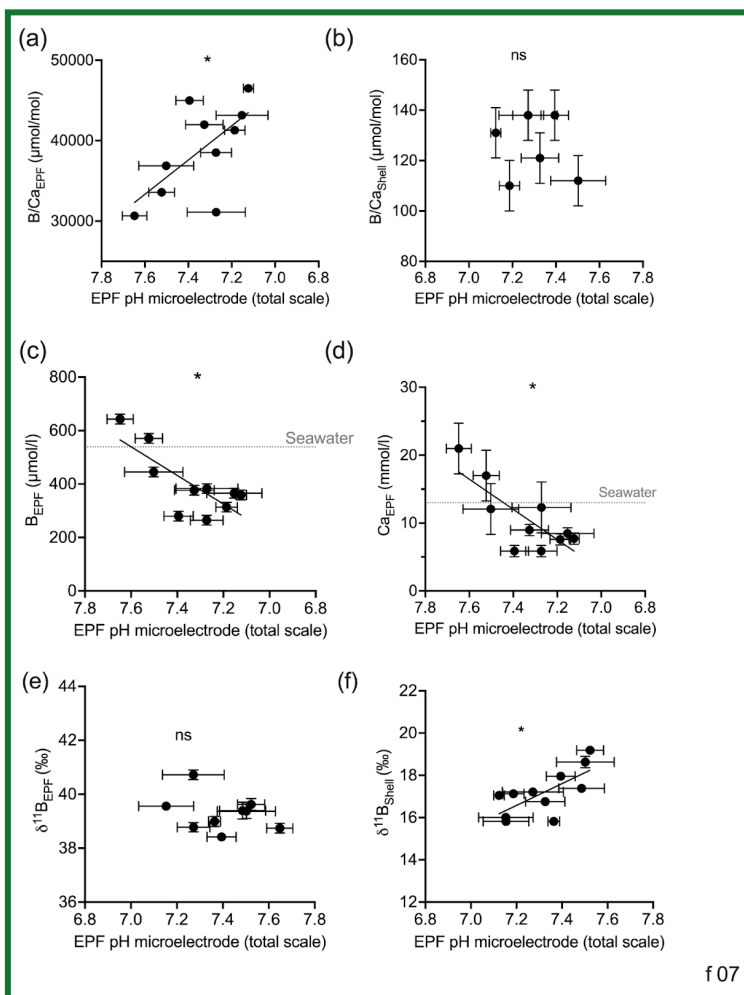
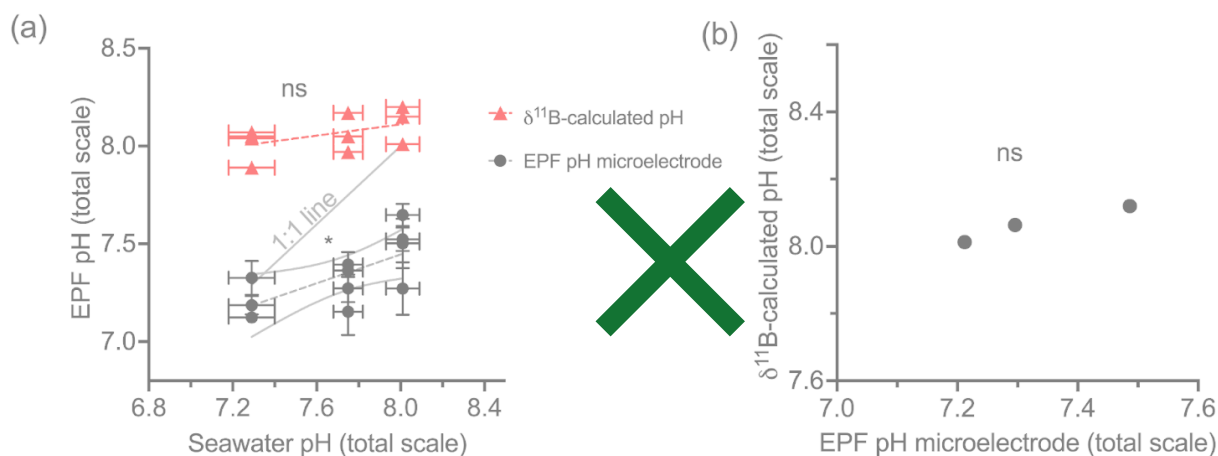


**Figure 7.** Scatter plots showing *C. virginica* individual specimen (a) EPF B/Ca and (b) shell B/Ca across corresponding microelectrode EPF pH. Additionally, scatter plots of (c) EPF B, (d) EPF  $\text{Ca}^{2+}$ , (e) EPF  $\delta^{11}\text{B}$ , and (f) shell  $\delta^{11}\text{B}$  across microelectrode EPF pH. Dotted gray lines on (c) and (d) show the average B and  $\text{Ca}^{2+}$  seawater concentration, respectively. Stars denote statistically significantly nonzero regression slopes and ‘ns’ signify non significant regressions (at significance  $p < 0.05$ ).



f 08

596

597

Figure 810. (a) Scatter plot of  $\delta^{11}\text{B}$ -calculated pH and microelectrode EPF pH across seawater pH treatments. The gray line shows the 1:1 seawater to EPF pH line. In the seawater pH: EPF pH space, the  $\delta^{11}\text{B}$ -calculated pH regression line is statistically nonzero (at significance  $p < 0.05$ ), with a slope of 0.368. The microelectrode EPF pH line was not significantly nonzero and had a slope of 0.143. (b) shows the averaged  $\delta^{11}\text{B}$ -calculated pH versus microelectrode EPF pH. Stars denote statistically significantly nonzero regression slopes and 'ns' signify non-significant regressions (at significance  $p < 0.05$ ).

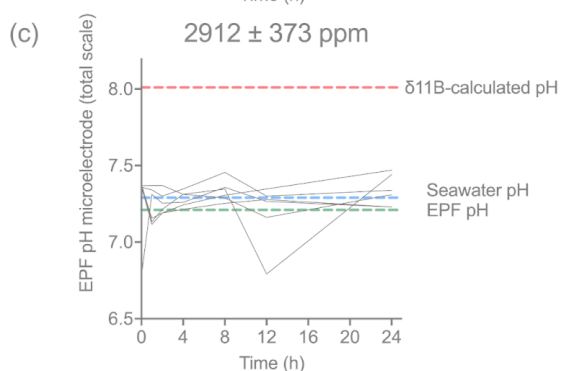
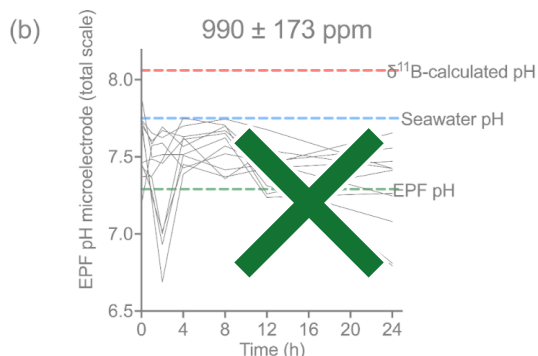
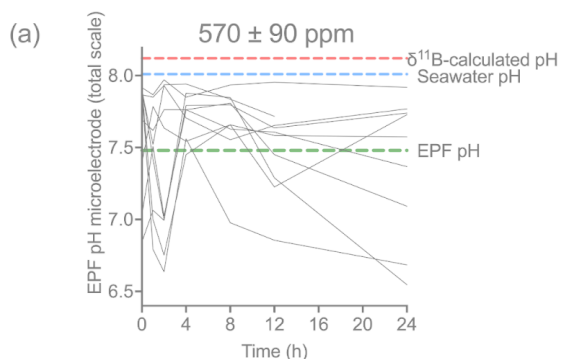
Fig 8a shows the measured EPF pH, the  $\delta^{11}\text{B}$ -calculated EPF, and seawater to EPF 1:1 pH line graphed across the *C. virginica* acidification experiment. The slope of the measured microelectrode EPF pH versus seawater pH linear regression was 0.3, and lies below the seawater to EPF 1:1 pH line, but intersects the seawater to EPF 1:1 pH line at lowest pH/highest  $p\text{CO}_2$  culture conditions (Fig 8). Conversely, the slope of the  $\delta^{11}\text{B}$ -calculated EPF pH versus seawater pH linear regression was 0.1, lies above the seawater to EPF 1:1 pH line, but intersected the seawater to EPF 1:1 pH line at higher culture pH conditions (Fig 8).

609

f 08

610 **Figure 8.** (a) Scatter plot of  $\delta^{11}\text{B}$ -calculated pH and microelectrode EPF pH across seawater pH treatments. The gray line  
 611 shows the 1:1 seawater to EPF pH line. The  $\delta^{11}\text{B}$ -calculated pH regression line had a slope of 0.14. The microelectrode EPF  
 612 pH line had a slope of 0.36. (b) shows the averaged  $\delta^{11}\text{B}$ -calculated pH versus microelectrode EPF pH. The 'ns' signifies a  
 613 non significant regression (at significance  $p < 0.05$ ).

614



f 09

615

616 Figure 911. Time series (in hours) of microelectrode EPF pH over a 24 hour period for (a) control (b) moderate and (c) high  
 617  $p\text{CO}_2$  treatments. Each line represents the microelectrode EPF pH for each individual specimen measured in that treatment.  
 618 The small dotted line shows the corresponding average  $\delta^{11}\text{B}$ -calculated pH for the treatment and the larger dotted line shows  
 619 the average seawater pH for the treatment.

620 For the *C. virginica* acidification experiment, Downey-Wall et al., (2020) measured the EPF pH of individual specimens in  
 621 each acidification treatment over a 24-hour period ( $n_{\text{total}}=108$  and  $n=6$  per time point per treatment). Fig 911 shows how the  
 622 EPF pH for each individual fluctuated over 24 hours. Ambient treatment EPF pH ranged from 6.63-7.94, moderate OA  
 623 treatment ranged from 6.68-7.88, and high OA treatment ranged from 6.78-7.47. The control treatment EPF pH of



individuals did intersect the averaged seawater pH for the treatment tanks, however, the EPF pH in the moderate and high pH treatments fell below the corresponding average treatment seawater pH lines. For all treatments, the time series EPF pH lines fell below the corresponding treatment averaged  $\delta^{11}\text{B}$ -calculated EPF pH line.

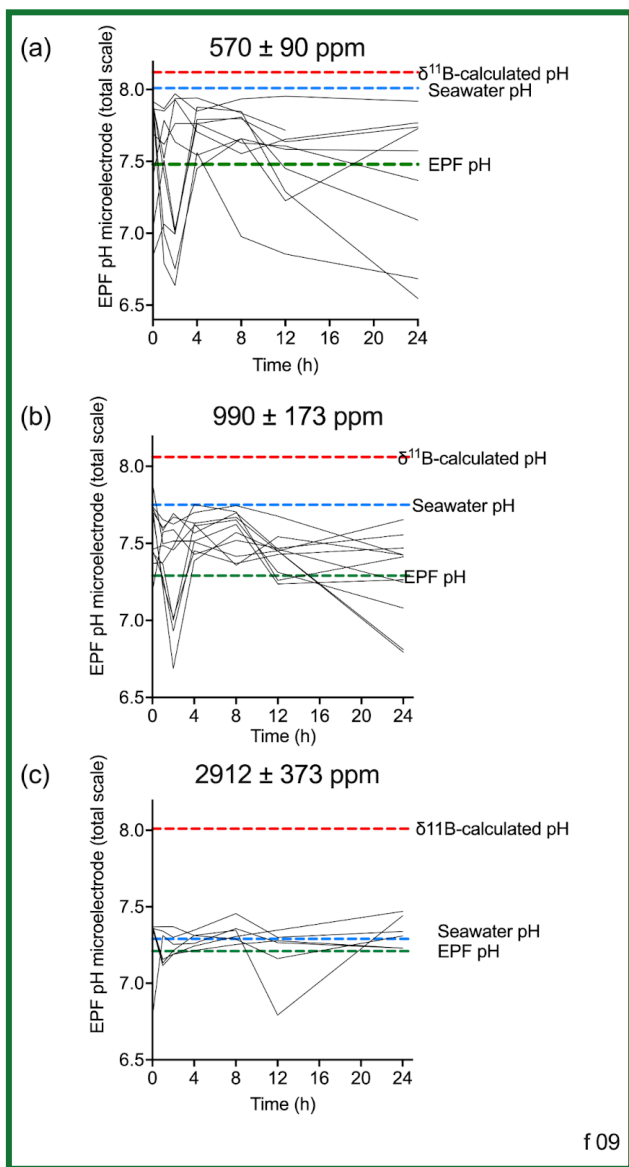


**Figure 9.** Time series (in hours) of microelectrode EPF pH over a 24 hour period for (a) control (n=10) (b) moderate (n=11) and (c) high  $p\text{CO}_2$  treatments (n=6). Each line represents the microelectrode EPF pH for each individual specimen measured in that treatment. The red dotted line shows the corresponding average  $\delta^{11}\text{B}$ -calculated pH for the treatment, the blue dotted line shows the average seawater pH for the treatment, and the green dotted line shows average EPF pH.

## 632 4. Discussion

### 633 4.1 Comparison of *A. islandica* and *C. virginica* $Mg^{2+}$ and $Ca^{2+}$ geochemistry of seawater, EPF, and bivalve shell

#### 634 ~~4.1 Comparison of *A. islandica* and *C. virginica* geochemistry of seawater, EPF, and bivalve shell~~

##### 635 ~~4.1.1 Elemental ratios and $[Mg^{2+}]$ and $[Ca^{2+}]$ concentrations in the EPF and shell~~

636 This study examined tripartite element and isotope fractionation between different reservoirs involved in the  
637 biomineralization of two bivalves species, aragonitic *A. islandica* and calcitic *C. virginica*. Marine bivalves source ions for  
638 internal fluids from seawater and previous studies by Crenshaw (1972) have highlighted that the extrapallial fluid, the  
639 internal ion reservoir pool for calcification, is chemically different from seawater. Seawater enters the hemolymph fluid  
640 within the bivalve tissues through the gills, filter feeding, and passive diffusion. Thereafter, the ions sourced from seawater  
641 are modulated either passively or actively across the outer mantle epithelium (OME) cells into the extrapallial cavity, a  
642 semi-isolated space that separates the outer mantle epithelium tissue from the shell. Here, ions are sourced to the site of  
643 calcification where biomineralization occurs. The exact mechanisms behind bivalve biomineralization is still a topic of  
644 active research and evidence has been put forth for several distinct pathways, primarily regulation of calcification  
645 constituents across the OME and transport of a precursor phase of  $CaCO_3$  to promote calcification (Addadi 2003; Checa  
646 2018).

647 In this study we found that the extrapallial fluid is chemically distinct from seawater. Here we show that, under  
648 ambient conditions, both the EPF  $Mg/Ca$  and  $B/Ca$  of both *C. virginica* and *A. islandica* were lower than that of seawater,  
649 indicating that the EPF has a distinct geochemical make up different from seawater (Fig 3; Downey-Wall et al., 2022). This  
650 is consistent with the anatomical understanding in bivalves that EPF is semi-isolated from seawater and its geochemistry can  
651 be influenced by ion fluxes across the OME as well as other ion pathways (Crenshaw 1972; Stemmer et al., 2019; Sillanpaa  
652 et al., 2018). However, we also find that for both  $Mg/Ca$  and  $B/Ca$ , this result is driven by an increase in absolute  $Ca^{2+}$  in  
653 EPF, so we do not find evidence for dilution or concentration of the absolute  $Mg^{2+}$  or  $B$  in the EPF (Fig 3). Previous work  
654 on bivalves has shown that magnesium can inhibit calcite crystal nucleation and there is evidence for exclusion of  $Mg^{2+}$   
655 from the EPF (Lorens and Bender, 1977). In line with other studies, we show that *C. virginica* and *A. islandica* have lower  
656  $Mg/Ca$  in EPF than seawater (Lorens and Bender, 1977; Planchon et al., 2013); however, we note that the EPF  $Mg/Ca$  trend  
657 is driven by changes in EPF  $Ca^{2+}$ . *C. virginica* and *A. islandica* EPF  $Mg/Ca$  were significantly different, with lower EPF  
658  $Mg/Ca$  for *A. islandica*, possibly due to different controls over EPF  $Ca^{2+}$  between both species. The partition coefficient  
659 between EPF and the shell was calculated to be 0.003 for *C. virginica* 0.0002 for *A. islandica*, which is consistent with  
660 previous studies on bivalves and with the  $Mg/Ca$  mineralogical difference between the calcite produced by *C. virginica* and  
661 the aragonite produced by *A. islandica* (Ulrich et al. 2021).

662 ~~Additionally, under ambient control conditions *C. virginica* and *A. islandica* microelectrode EPF pH was lower than~~  
663 ~~seawater pH. Additionally, under both the moderate and high experimental ocean acidification treatments, the average~~  
664 ~~microelectrode EPF pH of *C. virginica* was lower than seawater pH. These findings are in line with previous work on~~

bivalves, which show that the EPF pH is regularly lower than seawater pH (Crenshaw 1972; Heinemann et al., 2012; Stemmer et al., 2013; Sutton et al., 2018; Cameron et al. 2019; Liu et al., 2020).

We found that the EPF  $\delta^{26}\text{Mg}$  of *C. virginica* was depleted compared to seawater  $\delta^{26}\text{Mg}$  (Fig 3). Our  $\delta^{26}\text{Mg}$  values for the EPF and shell were in line with previous work on bivalves (Planchon et al., 2013). Planchon et al. (2013) found a  $-0.23 \pm 0.25 \text{ ‰}$  (2 SD,  $n=5$ ) difference between EPF and seawater in the aragonitic manila clam, *Ruditapes philippinarum*. Similarly, in the present study, a difference of  $-0.11 \pm 0.06 \text{ ‰}$  was observed for the calcitic *C. virginica*, but no  $\delta^{26}\text{Mg}$  data were collected for *A. islandica* due to sample limitation. Both Planchon et al. (2013) and the present study show depleted EPF  $\delta^{26}\text{Mg}$  relative to seawater  $\delta^{26}\text{Mg}$ , indicating a potential biological modulation of EPF  $\text{Mg}^{2+}$  which has been previously attributed to heavier isotopes being incorporated into soft tissues or magnesium fixation within organic molecules (Planchon et al., 2013). However, it is important to note that the difference between EPF and seawater  $\delta^{26}\text{Mg}$  is low and the  $\delta^{26}\text{Mg}$  fractionation between the shell and seawater (2.43‰) was slightly larger than but still in line with inorganic calcite precipitation studies (Mavromatis et al., 2013; Saulnier et al., 2012).

#### 4.2 Comparison of *A. islandica* and *C. virginica* EPF pH and boron geochemistry of seawater, EPF, and bivalve shell

The boron isotopes and B/Ca proxies have been used as paleo-pH and  $\text{CO}_3^{2-}$  proxies, respectively, recording changes in seawater carbonate chemistry in the shells of foraminifera (Hemming and Hanson 1992; Sanyal et al., 2001; Foster and Rae 2016). In different taxa corals, however, there is evidence that these proxies monitor changes in the carbonate chemistry of the internal calcifying fluid, which may be different from seawater geochemistry (Allison and Finch 2010; Cornwall et al., 2017; Sutton et al., 2018; Guillermic et al., 2021). The boron isotopes proxy has also been applied to other marine species (Sutton et al., 2018; Liu et al., 2020; Cornwall et al., 2017), but independent measurements are needed to fully understand the systematics of this proxy in other organisms. In the present study, we constrained the B/Ca and  $\delta^{11}\text{B}$  of the main reservoirs involved in the biomineralization (seawater, extrapallial fluid, and shell) of two species of bivalves, the oyster *C. virginica* and the clam *A. islandica*.

We found an incongruence between seawater pH, measured EPF pH and  $\delta^{11}\text{B}$ -calculated pH. For both *C. virginica* and *A. islandica* microelectrode EPF pH was lower than seawater pH. These findings are similar to previous work on bivalves which also show that the EPF pH is lower than seawater pH (Crenshaw 1972; Heinemann et al., 2012; Stemmer et al., 2019; Cameron et al. 2019). Microelectrode EPF pH between species was found to not be significantly different, indicating a similar downregulation in pH compared to seawater. However, our  $\delta^{11}\text{B}$ -based EPF pH was different between species (Fig 5). Using boron isotope systematics, this translated to a  $\delta^{11}\text{B}$ -calculated EPF pH of  $7.76 \pm 0.07$  for *A. islandica* and  $8.12 \pm 0.09$  for *C. virginica*. Although boron isotopes have been shown to probe the internal calcification fluid of certain taxa, like corals (e.g. Allison and Finch 2010), our results show an incongruence between measured EPF pH and  $\delta^{11}\text{B}$ -calculated pH.

#### 4.3 *C. virginica* ocean acidification effects on $\text{Mg}^{2+}$ and $\text{Ca}^{2+}$ geochemistry of seawater, EPF, and bivalve shell

699 In the complementary study by Downey-Wall et al. (2020), it was found that the *C. virginica* calcification rates  
700 decreased with seawater pH (Downey-Wall et al., 2020; Fig 2). The reduction of calcification under ocean acidification  
701 conditions is well documented in other seawater pH experiments on different bivalve species (e.g., Ries et al., 2009; Beniash  
702 et al., 2010; Waldbusser et al., 2011; Downey-Wall et al., 2020). This result is consequential as the shell is important in  
703 protecting the animal from predation, desiccation, and the effects of transient changes in seawater chemistry (Gosling et al.,  
704 2008). Under ocean acidification treatments, the average microelectrode EPF pH of *C. virginica* was lower than seawater  
705 pH. This is in line with other simulated ocean acidification studies that also found a decrease in EPF pH (Michaelidis et al.,  
706 2005; Thomsen et al., 2013; Zittier et al., 2015; Cameron et al., 2019; Downey-Wall et al., 2020). However, the change in pH  
707 between EPF and seawater pH ( $\Delta$ pH) decreased with decreasing pH, resulting in an EPF pH that was closer to seawater pH  
708 under acidified conditions (Fig 8a, Fig. 9c).

709 Only *C. virginica* was cultured under ocean acidification (OA) treatments representing control, moderate, and high  
710 OA treatments. As mentioned above, the control experiment showed elevation of EPF  $\text{Ca}^{2+}$  and EPF  $\text{Mg}^{2+}$  relative to  
711 seawater. However, as EPF pH decreased, the EPF  $\text{Ca}^{2+}$  and  $\text{Mg}^{2+}$  significantly decreased as well (Fig 6). Ion transporters  
712 such as voltage gated  $\text{Ca}^{2+}$ -channels tend to also affect chemically similar ions like  $\text{Mg}^{2+}$  and a reduction of such a transporter  
713 could possibly explain the similar trends in  $\text{Ca}^{2+}$  and  $\text{Mg}^{2+}$  concentrations under OA (Hess et al., 1986). Under OA  
714 conditions, EPF  $\text{Ca}^{2+}$  decreased to concentrations that were similar to or below seawater  $\text{Ca}^{2+}$ , indicating a reduced ability of  
715 the organism to upregulate these ions under OA conditions. Previous studies have found a similar tight coupling between pH  
716 and  $\text{Ca}^{2+}$ . For example, Stemmer et al. (2019) found synchronous patterns between pH and  $\text{Ca}^{2+}$  dynamics in *A. islandica* that  
717 they explained to be the result of calcium-transporting ATPase, which exchanges protons and calcium ions across the mantle  
718 and has proven to be important for acid-base regulation and calcium transport in bivalves (Stemmer et al., 2019; Sillanpaa et  
719 al., 2018; Sillanpaa et al., 2020). Although calcium transporting ATPase could explain this increase in  $\text{Ca}^{2+}$  under ambient  
720 conditions, this transport mechanism may be reduced under acidified conditions, thereby impairing the bivalve's ability to  
721 regulate protons and calcium ions in the extrapallial fluid, rendering EPF  $\text{Ca}^{2+}$  and pH more similar to that of seawater.

722 Alternatively, the simultaneous reduction in  $\text{Ca}^{2+}$  and  $\text{Mg}^{2+}$  under OA conditions could point to an ion storage  
723 mechanism. The reduction of both calcium and magnesium within the EPF under moderate and high OA treatments could  
724 possibly be linked to changes of storage and budgets of ions under stressful conditions (Mount et al., 2004; Johnstone et al.,  
725 2015; Wang et al. 2017). Further, several studies have highlighted significant changes in bivalve  $\text{Ca}^{2+}$  ion transport and  
726 storage in different extracellular and subcellular compartments associated with shell damage and repair under acidified  
727 conditions (Sillanpaa et al., 2016; Mount et al., 2004; Fitzer et al., 2016). Lastly, the EPF  $\text{Ca}^{2+}$  could simply reflect the  
728 balance between calcification and dissolution of the shell, as exemplified in a study on *C. virginica* conducted by Ries et al.  
729 (2016) which found that under similarly low saturation states, localized shell calcification was maintained despite net  
730 dissolution of the shell. Regardless of the exact mechanism, the reduction in extrapallial fluid  $\text{Ca}^{2+}$  under ocean acidification  
731 is a significant result that could impact the ability of bivalves to calcify by decreasing the  $\text{CaCO}_3$  saturation state of the EPF.

#### 732 4.4 *C. virginica* ocean acidification effects on boron geochemistry

733 Similarly to ambient conditions, the calculated  $\delta^{11}\text{B}$ -based pH for *C. virginica* is systematically higher than  
734 microelectrode EPF pH (Fig 8). Both  $\delta^{11}\text{B}$ -based pH and measured EPF pH record a decrease in pH under acidified  
735 conditions (regression  $p < 0.05$  for microelectrode pH). However, the offset between microelectrode EPF pH and the  
736  $\delta^{11}\text{B}$ -calculated pH was 0.3 pH units and increased to 0.6 and 0.8 pH units for the moderate and high OA treatments,  
737 respectively (Fig 8). This demonstrates that, under OA conditions, the incongruence between  $\delta^{11}\text{B}$  based pH and measured  
738 EPF pH increases and potentially renders the seawater pH proxy impractical, even after species-specific empirical  
739 calibration. Under OA conditions, shell  $\delta^{11}\text{B}$  was not correlated with changes in seawater pH, but was significantly correlated  
740 to microelectrode pH (Fig 7f). These data indicate that microelectrode EPF pH does not fully resolve  $\delta^{11}\text{B}$  vital effects or  
741 discrepancies.

742 However it is important to note the differences in timescales associated with  $\delta^{11}\text{B}$ -calculated EPF pH and  
743 microelectrode pH. Our microelectrode pH measurements, although averaged across several time points, show snapshots in  
744 time and are variable due different behavioral scenarios such as open (feeding, high pH) and closed (respiring into a closed  
745 system, low pH) cycles. Conversely, the  $\delta^{11}\text{B}$  approach represents EPF pH integrated average EPF pH over the interval that  
746 the sampled shell was formed, which could range from days to weeks. Furthermore, the  $\delta^{11}\text{B}$  method will only record EPF  
747 pH at the site of calcification when the shell is forming, which can skew the archiving of the  $\delta^{11}\text{B}$  pH signal in the shell to  
748 higher values because the crystal only forms when saturation states and calcification rates are higher. This potential bias is  
749 also consistent with our  $\delta^{11}\text{B}$ -calculated EPF pH data being higher than the microelectrode pH data, and similar to trends  
750 seen in corals (Cameron et al, 2022).

751 A possible explanation for the incongruence between  $\delta^{11}\text{B}$ -based pH and measured EPF pH arises from boron  
752 isotope systematics. The boron isotope proxy assumes that only the charged borate ion is incorporated as  $\text{BO}_4$  into the  
753 mineral but has been shown that boric acid can also be incorporated as  $\text{BO}_3$ , and NMR studies have shown the presence of  
754  $\text{BO}_3$  in the shells of different marine organisms (Rollion Bard et al., 2011; Cusack et al., 2015). However, the presence of  
755  $\text{BO}_3$  does not obviously translate to a strong bias in the  $\delta^{11}\text{B}$  signature of the mineral due to the potential re-coordination of  
756  $\text{BO}_4$  to  $\text{BO}_3$  within the crystal lattice (Klochko et al., 2009). A simple calculation shows that 14-17% boric acid incorporation  
757 could explain the observed difference between EPF pH and  $\delta^{11}\text{B}$ -calculated pH for *C. virginica*, which could very well  
758 explain the discrepancy. Alternatively, shell  $\delta^{11}\text{B}$  could also be affected by seawater or extrapallial fluid DIC, which bivalves  
759 are known to modulate under ambient and OA conditions (Crenshaw 1972, Stemmer et al., 2019). Gagnon et al. (2021)  
760 found that the shell  $\delta^{11}\text{B}$  of deep-water coral is independently sensitive to changes in seawater DIC as a result of diffusion of  
761 boric acid (Gagnon et al., 2021), though no similar studies have looked at the same effect in bivalves this mechanism is still  
762 possible. Taken together, these findings could explain the offset between  $\delta^{11}\text{B}$ -based pH and seawater or EPF pH.  
763 Nevertheless, this remains speculative as there is no further evidence of boric acid incorporation in these species.

764 The difference between microelectrode EPF pH and  $\delta^{11}\text{B}$ -based EPF pH implies that pH measured with boron  
765 isotopes probes a localized site of calcification rather than the entire EPF pool measured with microelectrode. A spatial and  
766 temporal study conducted by Stemmer et al. (2019) measured the EPF of *Arctica islandica* and showed highly dynamic

changes in pH,  $\text{Ca}^{2+}$  and DIC from the surface of the shell to the outer mantle epithelium (OME), with localized environment at the OME reaching pH values up to 9.5. Due to this high variability, it is possible that the EPF microelectrode measurements in this study did not capture the full variability of the EPF. Stemmer et al. (2019) presented EPF pH values measured at the shell surface ranging [7.1-7.6] for *A. islandica*, comparable to the values measured from microelectrode in this study (Fig 9). Additionally, Stemmer et al. (2019) found large influxes of DIC which could not have been explained just from metabolic activity, but instead indicated intense DIC pumping and bursts of calcification. These findings are in line with the holistic view of biomineralization outlined in Checa (2018) and Johnstone (2015) which argue that crystal deposition is a series of periodic events under biological regulation. In our study, a time-series of microelectrode EPF pH shows that at no point, during ventilation and closed cycles, does the EPF pH reach the  $\delta^{11}\text{B}$ -calculated pH (Fig 9). The fact that microelectrode EPF pH is systematically lower than seawater pH for both of our bivalve species may reflect localized differences in pH associated with zones of calcification. The two environments (site of calcification and bulk EPF) can act distinctly, with low pH and high DIC EPF being a source of carbon for the site of calcification in the bulk EPF, and elevated pH of the site of calcification supporting the conversion of the DIC species to  $[\text{CO}_3^{2-}]$  in support of mineral precipitation. Further work would be needed to assess this highly dynamic and localized environment, however our study shows that boron isotopes may reflect the pH of the microenvironment where calcification occurs within the EPF, which has previously been inferred by prior studies using non-geochemical approaches (Ramesh et al., 2017; Ramesh et al., 2018; Stemmer et al., 2019).

~~In the complementary study by Downey Wall et al. (2020), it was found that the *C. virginica* calcification rates decreased with seawater pH (Downey Wall et al., 2020; Fig 2). The reduction of calcification under ocean acidification conditions is well documented in other seawater pH experiments on different bivalve species (e.g., Ries et al., 2009; Beniash et al., 2010; Waldbusser et al., 2011; Downey Wall et al., 2020). This result is consequential as the shell is important in protecting the animal from predation, desiccation, and the effects of transient changes in seawater chemistry (Gosling 2008). Under ambient control conditions, *C. virginica* and *A. islandica* microelectrode EPF pH was lower than seawater pH. Additionally, under both the moderate and high experimental ocean acidification treatments, the average microelectrode EPF pH of *C. virginica* was lower than seawater pH. These findings are in line with previous work on bivalves, which show that the EPF pH is regularly lower than seawater pH (Crenshaw 1972, Heinemann et al., 2012, Stemmer et al., 2019, Sutton et al., 2018; Cameron et al. 2019, Liu et al., 2020) and that simulated ocean acidification results in a decreased EPF pH (Michaelidis et al., 2005; Thomsen et al., 2013, Zittier et al., 2015, Cameron et al., 2019; Downey Wall et al., 2020). However, the change in pH between EPF and seawater pH ( $\Delta\text{pH}$ ) decreased with decreasing pH, resulting in an EPF pH that was closer to seawater pH under acidified conditions (Table 1).~~

~~Here we show that, under ambient conditions, both the EPF Mg/Ca and B/Ca of both *C. virginica* and *A. islandica* were lower than that of seawater, indicating that the EPF has a distinct geochemical make up different from seawater (Fig 3; Downey Wall et al., 2022). This is consistent with the anatomical understanding in bivalves that EPF is semi-isolated from seawater and its geochemistry can be influenced by ion fluxes across the OME as well as other ion pathways (Crenshaw~~



1972; Stemmer et al., 2013; Sillanpaa et al., 2018). However, we also find that for both Mg/Ca and B/Ca, this result is driven by an increase in absolute  $[Ca^{2+}]$  in EPF, so we do not find evidence for dilution or concentration of the absolute  $[Mg^{2+}]$  or B in the EPF (Fig 3). Previous work on bivalves has shown that magnesium can inhibit calcite crystal nucleation and there is evidence for exclusion of  $[Mg^{2+}]$  from the EPF (Lorens and Bender, 1977). In line with other studies, we show that *C. virginica* and *A. islandica* have lower Mg/Ca in EPF than seawater (Lorens and Bender, 1977; Planchon et al., 2013); however, we note that the EPF Mg/Ca trend is driven by changes in EPF Ca. *C. virginica* and *A. islandica* EPF Mg/Ca were significantly different, with lower EPF Mg/Ca for *A. islandica*, possibly due to different controls over EPF  $[Ca^{2+}]$  between both species. The partition coefficient between EPF and the shell was calculated to be 0.003 for *C. virginica* 0.0002 for *A. islandica*, which is consistent with previous studies on bivalves and with the Mg/Ca mineralogical difference between the calcite produced by *C. virginica* and the aragonite produced by *A. islandica* (Ulrich et al. 2021).¶

We found that the EPF  $\delta^{26}Mg$  of *C. virginica* was depleted compared to seawater  $\delta^{26}Mg$  (Fig 3). Our  $\delta^{26}Mg$  values for the EPF and shell were in line with previous work on bivalves (Planchon et al., 2013). Planchon et al. (2013) found a  $-0.23 \pm 0.25$  ‰ (2 SD, n = 5) difference between EPF and seawater in the aragonitic manila clam, *Ruditapes philippinarum*. Similarly, in the present study, a difference of  $-0.11 \pm 0.06$  ‰ was observed for the calcitic *C. virginica*, but no  $\delta^{26}Mg$  data were collected for *A. islandica* due to sample limitation. Both Planchon et al. (2013) and the present study show depleted EPF  $\delta^{26}Mg$  relative to seawater  $\delta^{26}Mg$ , indicating a potential biological modulation of EPF  $[Mg^{2+}]$  which has been previously attributed to heavier isotopes being incorporated into soft tissues or magnesium fixation within organic molecules (Planchon et al., 2013). However, it is important to note that the difference between EPF and seawater  $\delta^{26}Mg$  is low and the  $\delta^{26}Mg$  fractionation between the shell and seawater (2.43‰) was slightly larger than but still in line with inorganic calcite precipitation studies (Mavromatis et al., 2013; Saulnier et al., 2012).¶

Only *C. virginica* was cultured under ocean acidification (OA) treatments representing control, moderate, and high OA treatments. As mentioned above, the control experiment showed elevation of EPF  $[Ca^{2+}]$  and EPF  $[Mg^{2+}]$  relative to seawater. However, as EPF pH decreased, the EPF  $[Ca^{2+}]$  and  $[Mg^{2+}]$  significantly decreased as well (Fig 3 & 65). Ion transporters such as voltage-gated  $Ca^{2+}$  channels tend to also affect chemically similar ions like  $[Mg^{2+}]$  and a reduction of such a transporter could possibly explain the similar trends in  $[Ca^{2+}]$  and  $[Mg^{2+}]$  concentrations under OA (Hess et al., 1986). Under OA conditions, EPF  $[Ca^{2+}]$  decreased to concentrations that were similar to or below seawater  $Ca^{2+}$ , indicating a reduced ability of the organism to upregulate these ions under OA conditions. Previous studies have found a similar tight coupling between pH and  $Ca^{2+}$ . For example, Stemmer et al. (20193) found synchronous patterns between pH and  $[Ca^{2+}]$  dynamics in *A. islandica* that they explained to be the result of calcium-transporting ATPase, which exchanges protons and calcium ions across the OME and has proven to be important for acid-base regulation and calcium transport in bivalves (Stemmer et al., 20193; Sillanpaa et al., 2018; Sillanpaa et al., 2020). Although calcium transporting ATPase could explain this increase in  $[Ca^{2+}]$  under ambient conditions, this transport mechanism may be reduced under acidified conditions, thereby impairing the bivalve's ability to regulate protons and calcium ions in the extrapallial fluid, rendering EPF  $[Ca^{2+}]$  and pH more similar to that of seawater.¶

Alternatively, the simultaneous reduction in  $[Ca^{2+}]$  and  $[Mg^{2+}]$  under OA conditions could point to an ion storage mechanism. The reduction of both calcium and magnesium within the EPF under moderate and high OA treatments could possibly be linked to changes of storage and budgets of ions under stressful conditions (Mount 2004; Johnstone et al., 2015; Wang et al. 2017). Further, several studies have highlighted significant changes in bivalve  $[Ca^{2+}]$  ion transport and storage in different extracellular and subcellular compartments associated with shell damage and repair under acidified conditions (Sillanpaa et al., 2016; Mount et al., 2004; Fitzer et al., 2016). Lastly, the EPF  $[Ca^{2+}]$  could simply reflect the balance between calcification and dissolution of the shell, despite the decrease in calcification rate over the experimental period, as exemplified by a study on *C. virginica* conducted by Ries et al. (2016) that found that under similarly low saturation states, localized shell calcification was maintained despite net dissolution of the shell. Regardless of the exact mechanism, the reduction in extrapallial fluid  $[Ca^{2+}]$  under ocean acidification is a significant result that could impact the ability of bivalves to calcify by decreasing the  $CaCO_3$  saturation state of the EPF.

#### 4.2 Boron geochemistry

The boron isotopes and B/Ca proxies have been used as paleo pH and  $CO_3^{2-}$  proxies, respectively, recording changes in seawater carbonate chemistry in the shells of foraminifera (Hemming and Hanson 1992; Sanyal et al., 2001; Foster and Rae 2016). In different taxa corals, however, there is evidence that these proxies monitor changes in the carbonate chemistry of the internal calcifying fluid, which may be different from seawater geochemistry (Allison and Finch 2010; Cornwall et al., 2017; Sutton et al., 2018; Guillermic et al., 2021). The boron isotopes proxy has also been applied to other marine species (Sutton et al., 2018; Liu et al., 2020; Cornwall et al., 2017), but independent measurements are needed to fully understand the systematics of this proxy in other organisms. In the present study, we constrained the B/Ca and  $\delta^{11}B$  of the main reservoirs involved in the biomineralization (seawater, extrapallial fluid, and shell) of two species of bivalves, the oyster *C. virginica* and the clam *A. islandica*.

For both *A. islandica* and *C. virginica*, there were no significant changes nor correlation observed between  $\delta^{11}B$  of the EPF and seawater (Fig 46). Shell  $\delta^{11}B$  was significantly different between species, with *A. islandica* recording lower shell  $\delta^{11}B$  ( $15.26 \pm 0.41$  ‰) than *C. virginica* ( $18.34 \pm 0.59$  ‰). Using boron isotope systematics, the  $\delta^{11}B$ -based EPF pH was determined to be  $7.76 \pm 0.07$  for *A. islandica* and  $8.12 \pm 0.09$  for *C. virginica*. The  $\delta^{11}B$ -based pH was significantly different between the two species (t-test p value <0.05) and also significantly different from the direct EPF microelectrode pH measurements of  $7.41 \pm 0.14$  and  $7.48 \pm 0.15$  for *A. islandica* and *C. virginica*, respectively (t-test p value < 0.05). In other words, the use of canonical  $\delta^{11}B$  proxy systematics to calculate  $\delta^{11}B$ -based pH does not match direct measurements of EPF pH. Microelectrode EPF pH was consistently lower than seawater for both species.  $\delta^{11}B$ -based pH also revealed EPF pH lower than seawater pH for *A. islandica* (but to a lesser extent than direct microelectrode measurement), but an EPF pH greater than seawater for *C. virginica*. Similarly to ambient conditions, This observation in the control experiments holds true under ocean acidification, where the  $\delta^{11}B$ -based pH is systematically higher than microelectrode EPF pH (Fig 810). Both  $\delta^{11}B$ -based pH and measured EPF pH record a decrease in pH under acidified conditions (regression p<0.05 for



microelectrode pH). However, the offset between microelectrode EPF pH and the  $\delta^{11}\text{B}$ -calculated pH was 0.3 pH units and increased to 0.6 and 0.8 pH units for the moderate and high OA treatments, respectively (Table 21). This demonstrates that, under OA conditions, the incongruence between  $\delta^{11}\text{B}$ -based pH and measured EPF pH increases and potentially renders the seawater pH proxy impractical, even after species-specific empirical calibration. As seen in Figure 7f, shell  $\delta^{11}\text{B}$  was not correlated with seawater pH, but was significantly correlated to microelectrode pH. These data indicate that microelectrode EPF pH does not fully resolve  $\delta^{11}\text{B}$ -vital effects. However it is important to note the differences in timescales associated with  $\delta^{11}\text{B}$ -calculated EPF pH and microelectrode pH. Our microelectrode pH measurements, although averaged across several time points, show snapshots in time and are variable due to different behavioral scenarios such as open (feeding, high pH) and closed (respiring into a closed system, low pH) cycles. Conversely, the  $\delta^{11}\text{B}$  approach represents EPF pH integrated average EPF pH over the interval that the sampled shell was formed, which could range from days to weeks. Furthermore, the  $\delta^{11}\text{B}$  method will only record EPF pH when the shell is forming, which can skew the archiving of the  $\delta^{11}\text{B}$  (pH) signal in the shell to higher values because the crystal only forms when saturation states and calcification rates are higher. This potential bias is also consistent with our  $\delta^{11}\text{B}$ -calculated EPF pH data being higher than the microelectrode pH data, and similar to trends seen in the corals (Cameron et al., 2022).¶¶

A possible explanation for the incongruence between  $\delta^{11}\text{B}$ -based pH and measured EPF pH arises from boron isotope systematics. The boron isotope proxy assumes that only the charged borate ion is incorporated as  $\text{BO}_4$  into the mineral but has been shown that boric acid can also be incorporated as  $\text{BO}_3$ , and NMR studies have shown the presence of  $\text{BO}_3$  in the shells of different marine organisms (Rollion-Bard et al., 2011; Cusack et al., 2015). However, the presence of  $\text{BO}_3$  does not obviously translate to a strong bias in the  $\delta^{11}\text{B}$  signature of the mineral due to the potential re-coordination of  $\text{BO}_4$  to  $\text{BO}_3$  within the crystal lattice (Klochko et al., 2009). A simple calculation shows that 14–17% boric acid incorporation could explain the observed difference between EPF pH and  $\delta^{11}\text{B}$ -calculated pH for *C. virginica*, with only 6% boric acid incorporation needed for *A. islandica*, which could very well explain the discrepancy. Alternatively, shell  $\delta^{11}\text{B}$  could also be affected by seawater or extrapallial fluid DIC, which bivalves are known to modulate under ambient and OA conditions (Crenshaw 1972; Stemmer et al., 2019). Gagnon et al. (2021) found that the shell  $\delta^{11}\text{B}$  of deep-water coral is independently sensitive to changes in seawater DIC as a result of diffusion of boric acid (Gagnon et al., 2021), though no similar studies have looked at the same effect in bivalves this mechanism is still possible. Taken together, these findings could explain the offset between  $\delta^{11}\text{B}$ -based pH and seawater or EPF pH. Nevertheless, this remains speculative as there is no further evidence of boric acid incorporation in these species.¶¶

Furthermore, boron isotope derived pH can be influenced by diffusion of boric acid across cell membranes (Stoll et al., 2012; Liu et al., 2018; Liu et al., 2021; Gagnon et al., 2021). At two extremes, diffusion between seawater and the calcifying fluid pool can be fast, resulting in chemically and isotopic equilibrium between both pools, or diffusion can be slow, resulting in calcifying fluid being isolated from seawater such that the boron isotopes would record the chemistry of the calcifying fluid under physiological control. If diffusion is fast compared to other processes, then seawater and the calcifying fluid would be in equilibrium and the  $\delta^{11}\text{B}$  would not differ between the two pools. Our data show no difference

903 between seawater and EPF  $\delta^{11}\text{B}$ . However, differences in  $\text{Ca}^{2+}$ ,  $\text{Mg}^{2+}$ , and  $\delta^{26}\text{Mg}$  between seawater and EPF does provide  
904 evidence for physiological modulation of the EPF, despite similar  $\delta^{11}\text{B}$  signatures. ¶

905 In the case where there is not a strong diffusion of boric acid, then the pH calculated from boron isotopes should  
906 reflect the pH at the site of calcification and physiological control over the calcifying fluid. The difference between  
907 microelectrode EPF pH and  $\delta^{11}\text{B}$ -based EPF pH implies that pH measured with boron isotopes probes a localized site of  
908 calcification rather than the entire EPF pool measured with microelectrode. A spatial and temporal study conducted by  
909 Stemmer et al. (2019) measured the EPF of *Arctica islandica* and showed highly dynamic changes in pH,  $[\text{Ca}^{2+}]$  and DIC  
910 from the surface of the shell to the outer mantle epithelium (OME), with localized environment at the OME reaching pH  
911 values up to 9.5. Due to this high variability, it is possible that the EPF microelectrode measurements in this study did not  
912 capture the full variability of the EPF. Stemmer et al. (2019) presented EPF pH values measured at the shell surface ranging  
913 [7.1–7.6] for *A. islandica*, comparable to the values measured from microelectrode in this study. Additionally, Stemmer et al.  
914 (2019) found large influxes of DIC which could not have been explained just from metabolic activity, but instead indicated  
915 intense DIC pumping and bursts of calcification. These findings are in line with the holistic view of biomineralization  
916 outlined in Checa (2018) and Johnstone (2015) that argue that crystal deposition is a series of periodic events under  
917 biological regulation. In our study, a time-series of microelectrode EPF pH shows that at no point, during ventilation and  
918 closed cycles, does the EPF pH reach the  $\delta^{11}\text{B}$ -calculated pH (Fig. 911). The fact that microelectrode EPF pH is  
919 systematically lower than seawater pH for both of our bivalve species may reflect localized differences in pH associated with  
920 zones of calcification. The two environments (site of calcification and bulk EPF) can act distinctly, with low pH and high  
921 DIC EPF being a source of carbon for the site of calcification, and with the elevated pH of the site of calcification supporting  
922 the conversion of the DIC species to  $[\text{CO}_3^{2-}]$  in support of mineral precipitation. Further work would be needed to assess this  
923 highly dynamic and localized environment, however our study shows that boron isotopes may reflect the pH of the  
924 microenvironment where calcification occurs within the EPF, which has previously been inferred by prior studies using  
925 non-geochemical approaches (Ramesh et al., 2017; Ramesh et al., 2018; Stemmer et al., 2019). ¶

## 926 Conclusion

927 In this study, we used numerous approaches constraining the geochemical composition of and partitioning between  
928 the tripartite reservoirs of bivalve mineralization system--seawater, the EPF and the shell. Our study presents Mg/Ca and  
929 B/Ca, and absolute  $[\text{Ca}^{2+}]$  data of the seawater, EPF and shell. Comparisons of seawater and extrapallial fluid Mg/Ca and  
930 B/Ca,  $\text{Ca}^{2+}$ , and  $\delta^{26}\text{Mg}$  indicate that the EPF has a distinct composition that differs from seawater. Additionally, our OA  
931 experiments show that the EPF Mg/Ca and B/Ca, as well as absolute  $\text{Mg}^{2+}$ , B, and  $\text{Ca}^{2+}$ , all were significantly affected by  
932  $\text{CO}_2$ -induced ocean acidification, demonstrating that the biological pathways regulating or storing these ions involved in  
933 calcification are impacted by ocean acidification. Decreased calcium ion concentration within the extrapallial fluid due to  
934 OA could impair calcification by lowering the saturation state of the EPF with respect to  $\text{CaCO}_3$ . Additionally, our results

935 show that shell  $\delta^{11}\text{B}$  does not faithfully record seawater pH. However, shell  $\delta^{11}\text{B}$  is correlated with EPF pH, despite an offset  
936 from *in situ* microelectrode pH measurements. Both microelectrode pH and  $\delta^{11}\text{B}$ -calculated pH decreased with decreasing  
937 pH. However, the  $\delta^{11}\text{B}$ -calculated pH values were consistently higher than microelectrode pH measurements, indicating that  
938 the shell  $\delta^{11}\text{B}$  may reflect pH at a more localized site of calcification, rather than pH of the bulk EPF. Furthermore, the offset  
939 between the  $\delta^{11}\text{B}$ -calculated pH and microelectrode pH increased with decreasing pH under ocean acidification, indicating  
940 OA has a larger effect on bulk pH of the EPF measured via microelectrode than on site of calcification pH—the latter of  
941 which the bivalve may have more physiological control over to ensure continued calcification, even under chemically  
942 unfavorable conditions. These complex dynamics of EPF chemistry suggest that boron proxies in these two bivalve species  
943 are not straightforwardly related to seawater pH, precluding utilization of those species for reconstructing the carbonate  
944 chemistry of seawater. Moreover, the  $\delta^{11}\text{B}$  proxy may not be suitable for reconstructing seawater pH for bivalves with high  
945 physiological control over their internal calcifying fluid and is further complicated under conditions of moderate and extreme  
946 ocean acidification, where  $\delta^{11}\text{B}$  EPF pH deviates further from bulk microelectrode pH, possibly due to the effect of DIC on  
947 shell  $\delta^{11}\text{B}$  or the ~~tendency~~<sup>tendancy</sup> for shell  $\delta^{11}\text{B}$  to reflect EPF pH at the more localized site of calcification, rather than pH  
948 of the bulk EPF.

#### 949 **Author contribution**

950 LPC, AD, JBR, and KL designed the experiments and carried them out. BAC, MG, and RAE developed the geochemical  
951 study. BAC and MG performed geochemical analysis with the help of JNS and JAH. BAC, MG, and RAE prepared the  
952 manuscript with contributions from all co-authors.

#### 953 **Competing interests**

954 The authors declare that they have no conflict of interest.

#### 955 **Acknowledgements**

956 BAC was supported by the National Science Foundation Graduate Research Fellowship Program under Grant No.  
957 DGE-2034835 and the UC Eugene Cota-Robles Fellowship. BAC, MG, and RAE are supported by the Ocean Science work  
958 of Center for Diverse Leadership in Science which is funded by a grant from the David and Lucile Packard Foundation (no.  
959 85180), National Science Foundation grant NSF-RISE-2024426, and by gifts from Oceankind and Dalio Philanthropies. The  
960 Center for Diverse Leadership in Science is also supported by NSF-RISE-2228198, the Waverly Foundation, the Silicon  
961 Valley Community Foundation, and the Sloan Foundation. KL and JBR were supported by the National Science Foundation

962 grant BIO-OCE 1635423. The authors would like to thank Celine Liorzou, Yoan Germain, and Anne Trinquier for their  
963 technical support at the PSO. Additionally, the authors would like to thank Stefania Gili for her technical support at  
964 Princeton University.

965

## 966 References

- 967 1. Addadi, L., Raz, S., and Weiner, S.: Taking Advantage of Disorder: Amorphous calcium carbonate and its roles in  
968 biomineralization, *Advanced Materials*, 15, 959–970, 2003.
- 969 2. Addadi, L., Joester, D., Nudelman, F., and Weiner, S.: Mollusc Shell Formation: A Source of New Concepts for  
970 Understanding Biomineralization Processes, *Chemistry A European J*, 12, 980–987, 2006.
- 971 3. Ahm, A.-S. C., Bjerrum, C. J., Hoffman, P. F., Macdonald, F. A., Maloof, A. C., Rose, C. V., Strauss, J. V., and  
972 Higgins, J. A.: The Ca and Mg isotope record of the Cryogenian Trezona carbon isotope excursion, *Earth and*  
973 *Planetary Science Letters*, 568, 117002, 2021.
- 974 4. Alibert, C. and McCulloch, M. T.: Strontium/calcium ratios in modern *porites* corals From the Great Barrier Reef as  
975 a proxy for sea surface temperature: Calibration of the thermometer and monitoring of ENSO, *Paleoceanography*,  
976 12, 345–363, 1997.
- 977 5. Allison, N. and Finch, A. A.:  $\delta^{11}\text{B}$ , Sr, Mg and B in a modern *Porites* coral: the relationship between calcification  
978 site pH and skeletal chemistry, *Geochimica et Cosmochimica Acta*, 74, 1790–1800, 2010.
- 979 6. Barker, S., Greaves, M., and Elderfield, H.: A study of cleaning procedures used for foraminiferal Mg/Ca  
980 paleothermometry, *Geochemistry, Geophysics, Geosystems*, 4(9), 2003.
- 981 7. Beniash, E., Ivanina, A., Lieb, N. S., Kurochkin, I., and Sokolova, I. M.: Elevated level of carbon dioxide affects  
982 metabolism and shell formation in oysters *Crassostrea virginica*, *Marine Ecology Progress Series*, 419, 95–108,  
983 2010.
- 984 8. Broecker, W. S. and Peng, T.-H.: *Tracers in the Sea*, Lamont-Doherty Geological Observatory, Columbia University  
985 Palisades, New York, 1982.
- 986 9. Cameron, L. P., *Understanding Patterns of Bivalve Vulnerability and Resilience to Ocean Acidification: Insights*  
987 *from Field Studies, Tank Experiments and Novel Physiological Studies*, Dissertation Northeastern University, 2020.
- 988 10. Cameron, L.P., Reymond, C.E., Bijma, J., Büscher, J.V., de Beer, D., Guillermic, M., Eagle, R.A., Gunnell, J.,  
989 Müller-Lundin, F., Schmidt-Grieb, G.M., Westfield, I., Westphal, H., Ries, J.B., Impacts of warming and  
990 acidification on coral calcification linked to photosymbiont loss and deregulation of calcifying fluid pH, *Journal of*  
991 *Marine Science and Engineering*, 10, 1106, 2022.
- 992 11. Cameron, L. P., Grabowski, J. H., Ries, J. B., Impact of ocean acidification and warming on calcification rate,  
993 survival, extrapallial fluid chemistry, and respiration of the Atlantic sea scallop *Placopecten magellanicus*,  
994 *Limnology & Oceanography*, 1-17, 2019.

12. Checa, A. G.: Physical and Biological Determinants of the Fabrication of Molluscan Shell Microstructures, *Frontiers in Marine Science*, 5, 2018.
13. Cornwall, C. E., Comeau, S., and McCulloch, M. T.: Coralline algae elevate pH at the site of calcification under ocean acidification, *Global Change Biology*, 23, 4245–4256, 2017.
14. Craig, H.: The geochemistry of the stable carbon isotopes, *Geochimica et cosmochimica acta*, 3, 53–92, 1953.
15. Crenshaw, M. A.: The inorganic composition of molluscan extrapallial fluid, *The Biological Bulletin*, 143, 506–512, 1972.
16. Cusack, M., Kamenos, N. A., Rollion-Bard, C., and Tricot, G.: Red coralline algae assessed as marine pH proxies using 11B MAS NMR, *Scientific Reports*, 5, 8175, 2015.
17. Downey-Wall, A. M., Cameron, L. P., Ford, B. M., McNally, E. M., Venkataraman, Y. R., Roberts, S. B., Ries, J. B., and Lotterhos, K. E.: Ocean acidification induces subtle shifts in gene expression and DNA methylation in mantle tissue of the Eastern oyster (*Crassostrea virginica*), *Frontiers in Marine Science*, 7, 566419, 2020.
18. Dunbar, R. B., Wellington, G. M., Colgan, M. W., and Glynn, P. W.: Eastern Pacific sea surface temperature since 1600 A.D.: The  $\delta^{18}\text{O}$  record of climate variability in Galápagos Corals, *Paleoceanography*, 9, 291–315, 1994.
19. Eagle, R. A., Guillermic, M., De Corte, I., Alvarez Caraveo, B., Bove, C. B., Misra, S., Cameron, L. P., Castillo, K. D., and Ries, J. B.: Physicochemical Control of Caribbean Coral Calcification Linked to Host and Symbiont Responses to Varying  $p\text{CO}_2$  and Temperature, *Journal of Marine Science and Engineering*, 10, 1075, 2022.
20. Elderfield, H., Yu, J., Anand, P., Kiefer, T., and Nyland, B.: Calibrations for benthic foraminiferal Mg/Ca paleothermometry and the carbonate ion hypothesis, *Earth and Planetary Science Letters*, 250, 633–649, 2006.
21. Fitzer, S. C., Chung, P., Maccherozzi, F., Dhesi, S. S., Kamenos, N. A., Phoenix, V. R., and Cusack, M.: Biomineral shell formation under ocean acidification: a shift from order to chaos, *Scientific Reports*, 6, 21076, 2016.
22. Foster, G. L. and Rae, J. W. B.: Reconstructing Ocean pH with Boron Isotopes in Foraminifera, *Annual Review of Earth and Planetary Sciences*, 44, 207–237, 2016.
23. Gagnon, A. C., Gothmann, A. M., Branson, O., Rae, J. W. B., and Stewart, J. A.: Controls on boron isotopes in a cold-water coral and the cost of resilience to ocean acidification, *Earth and Planetary Science Letters*, 554, 116662, 2021.
24. Gaillardet, J., Lemarchand, D., Göpel, C., and Manhès, G.: Evaporation and Sublimation of Boric Acid: Application for Boron Purification from Organic Rich Solutions, *Geostandards Newsletter*, 25, 67–75, 2001.
25. Gazeau, F., Parker, L. M., Comeau, S., Gattuso, J.-P., O'Connor, W. A., Martin, S., Pörtner, H.-O., and Ross, P. M.: Impacts of ocean acidification on marine shelled molluscs, *Marine Biology*, 160, 2207–2245, 2013.
26. Gibson, R., Barnes, M., and Atkinson, R.: Molluscs as archives of environmental change, *Oceanography Marine Biology Annual Review*, 39, 103–164, 2001.

27. Gilbert, P., Bergmann, K. D., Boekelheide, N., Tambutté, S., Mass, T., Marin, F., Adkins, J. F., Erez, J., Gilbert, B., Knutson, V., Cantine, M., Hernández, J. O., and Knoll, A. H.: Biomineralization: Integrating mechanism and evolutionary history, *Science Advances*, 8, eabl9653, 2022.
28. Gosling, E.: *Bivalve molluscs: biology, ecology and culture*, John Wiley & Sons, 2008.
29. Guillermic, M., Cameron, L. P., De Corte, I., Misra, S., Bijma, J., De Beer, D., Reymond, C. E., Westphal, H., Ries, J. B., and Eagle, R. A.: Thermal stress reduces pocilloporid coral resilience to ocean acidification by impairing control over calcifying fluid chemistry, *Science Advances*, 7, eaba9958, 2021.
30. Gutjahr, M., Bordier, L., Douville, E., Farmer, J., Foster, G. L., Hathorne, E. C., Hönlisch, B., Lemarchand, D., Louvat, P., McCulloch, M., Noireaux, J., Pallavicini, N., Rae, J. W. B., Rodushkin, I., Roux, P., Stewart, J. A., Thil, F., and You, C.: Sub-Permil Interlaboratory Consistency for Solution-Based Boron Isotope Analyses on Marine Carbonates, *Geostandards and Geoanalytical Research*, 45, 59–75, 2021.
31. Heinemann, A., Fietzke, J., Melzner, F., Böhm, F., Thomsen, J., Garbe-Schönberg, D., and Eisenhauer, A.: Conditions of *Mytilus edulis* extracellular body fluids and shell composition in a pH-treatment experiment: Acid-base status, trace elements and  $\delta^{11}\text{B}$ , *Geochemistry Geophysics Geosystems*, 13, 2011GC003790, 2012.
32. Helm, M. M., Bourne, N., and Lovatelli, A.: *Hatchery culture of bivalves: a practical manual*, 2004.
33. Hemming, N. G. and Hanson, G. N.: Boron isotopic composition and concentration in modern marine carbonates, *Geochimica et Cosmochimica Acta*, 56, 537–543, 1992.
34. Hess, P., Lansman, J. B., & Tsien, R. W. Calcium channel selectivity for divalent and monovalent cations. Voltage and concentration dependence of single channel current in ventricular heart cells. *The Journal of general physiology*, 88(3), 293-319, 1986.
35. Higgins, J. A., Blättler, C. L., Lundstrom, E. A., Santiago-Ramos, D. P., Akhtar, A. A., Crüger Ahm, A.-S., Bialik, O., Holmden, C., Bradbury, H., Murray, S. T., and Swart, P. K.: Mineralogy, early marine diagenesis, and the chemistry of shallow-water carbonate sediments, *Geochimica et Cosmochimica Acta*, 220, 512–534, 2018.
36. Hönlisch, B., Hemming, Ng., Grottoli, A. G., Amat, A., Hanson, G. N., and Bijma, J.: Assessing scleractinian corals as recorders for paleo-pH: Empirical calibration and vital effects, *Geochimica et Cosmochimica Acta*, 68, 3675–3685, 2004.
37. Husson, J. M., Higgins, J. A., Maloof, A. C., and Schoene, B.: Ca and Mg isotope constraints on the origin of Earth's deepest  $\delta^{13}\text{C}$  excursion, *Geochimica et Cosmochimica Acta*, 160, 243–266, 2015.
38. Immenhauser, A., Schöne, B. R., Hoffmann, R., and Niedermayr, A.: Mollusc and brachiopod skeletal hard parts: Intricate archives of their marine environment, *Sedimentology*, 63, 1–59, 2016.
39. Johnstone, M. B., Gohad, N. V., Falwell, E. P., Hansen, D. C., Hansen, K. M., and Mount, A. S.: Cellular orchestrated biomineralization of crystalline composites on implant surfaces by the eastern oyster, *Crassostrea virginica* (Gmelin, 1791), *Journal of Experimental Marine Biology and Ecology*, 463, 8–16, 2015.



40. Klochko, K., Kaufman, A. J., Yao, W., Byrne, R. H., and Tossell, J. A.: Experimental measurement of boron isotope fractionation in seawater, *Earth and Planetary Science Letters*, 248, 276–285, 2006.
41. Klochko, K., Cody, G. D., Tossell, J. A., Dera, P., & Kaufman, A. J. Re-evaluating boron speciation in biogenic calcite and aragonite using <sup>11</sup>B MAS NMR. *Geochimica et Cosmochimica Acta*, 73(7), 1890–1900, 2009.
42. Kroeker, K. J., Micheli, F., Gambi, M. C., & Martz, T. R. Divergent ecosystem responses within a benthic marine community to ocean acidification. *Proceedings of the National Academy of Sciences*, 108(35), 14515–14520, 2011.
43. Liu, Y.-W., Sutton, J. N., Ries, J. B., and Eagle, R. A.: Regulation of calcification site pH is a polyphyletic but not always governing response to ocean acidification, *Science Advances*, 6, eaax1314, 2020.
44. Liu, Y.-W., Wanamaker Jr, A. D., Aciego, S. M., Searles, I., Hangstad, T. A., Chierici, M., and Carroll, M. L.: Resistant calcification responses of *Arctica islandica* clams under ocean acidification conditions, *Journal of Experimental Marine Biology and Ecology*, 560, 151855, 2023.
45. Lorens, R. B. and Bender, M. L.: Physiological exclusion of magnesium from *Mytilus edulis* calcite, *Nature*, 269, 793–794, 1977.
46. Mavromatis, V., Gautier, Q., Bosc, O., & Schott, J. Kinetics of Mg partition and Mg stable isotope fractionation during its incorporation in calcite. *Geochimica et Cosmochimica Acta*, 114, 188–203, 2013
47. McCulloch, M. T., D’Olivo, J. P., Falter, J., Holcomb, M., and Trotter, J. A.: Coral calcification in a changing world and the interactive dynamics of pH and DIC upregulation, *Nature Communications*, 8, 15686, 2017.
48. McCulloch, M. T., D’Olivo, J. P., Falter, J., Georgiou, L., Holcomb, M., Montagna, P., and Trotter, J. A.: Boron Isotopic Systematics in Scleractinian Corals and the Role of pH Up-regulation, in: *Boron Isotopes*, Springer International Publishing, Cham, 145–162, 2018.
49. McNally, E. M., Downey-Wall, A. M., Titmuss, F. D., Cortina, C., Lotterhos, K., and Ries, J. B.: Parental exposure of Eastern oysters ( *Crassostrea virginica* ) to elevated p CO<sub>2</sub> mitigates its negative effects on early larval shell growth and morphology, *Limnology & Oceanography*, 67, 1732–1745, 2022.
50. Michaelidis, B., Ouzounis, C., Paleras, A., and Pörtner, H. O.: Effects of long-term moderate hypercapnia on acid–base balance and growth rate in marine mussels *Mytilus galloprovincialis*, *Marine Ecology Progress Series*, 293, 109–118, 2005.
51. Mount, A. S., Wheeler, A. P., Paradkar, R. P., and Snider, D.: Hemocyte-Mediated Shell Mineralization in the Eastern Oyster, *Science*, 304, 297–300, 2004.
52. Nir, O., Vengosh, A., Harkness, J. S., Dwyer, G. S., and Lahav, O.: Direct measurement of the boron isotope fractionation factor: Reducing the uncertainty in reconstructing ocean paleo-pH, *Earth and Planetary Science Letters*, 414, 1–5, 2015.
53. Norrie, C. R., Dunphy, B. J., Ragg, N. L. C., & Lundquist, C. J. Ocean acidification can interact with ontogeny to determine the trace element composition of bivalve shell. *Limnology and Oceanography Letters*, 3(5), 393–400, 2018.

54. Orr, J. C., Fabry, V. J., Aumont, O., Bopp, L., Doney, S. C., Feely, R. A., ... & Yool, A. Anthropogenic ocean acidification over the twenty-first century and its impact on calcifying organisms. *Nature*, 437(7059), 681-686, 2005
55. Peharda, M., Schöne, B. R., Black, B. A., and Corregge, T.: Advances of sclerochronology research in the last decade, *Palaeogeography, Palaeoclimatology, Palaeoecology*, 570, 110371, 2021.
56. Pierrot, D. E., Wallace, D. W. R., and Lewis, E.: MS Excel program developed for CO<sub>2</sub> system calculations, Carbon dioxide information analysis center, 2011.
57. Planchon, F., Poulain, C., Langlet, D., Paulet, Y.-M., and André, L.: Mg-isotopic fractionation in the manila clam (*Ruditapes philippinarum*): New insights into Mg incorporation pathway and calcification process of bivalves, *Geochimica et cosmochimica acta*, 121, 374–397, 2013.
58. Raitzsch, M., Bijma, J., Bickert, T., Schulz, M., Holbourn, A., & Kučera, M. (2021). Atmospheric carbon dioxide variations across the middle Miocene climate transition. *Climate of the Past*, 17(2), 703-719.
59. Ramesh, K., Hu, M. Y., Thomsen, J., Bleich, M., & Melzner, F. Mussel larvae modify calcifying fluid carbonate chemistry to promote calcification. *Nature Communications*, 8(1), 1709, 2017.
60. Ramesh, K., Melzner, F., Griffith, A. W., Gobler, C. J., Rouger, C., Tasdemir, D., and Nehrke, G.: In vivo characterization of bivalve larval shells: a confocal Raman microscopy study, *Journal of the Royal Society Interface*, 15, 20170723, 2018.
61. Ries, J. B., Cohen, A. L., and McCorkle, D. C.: Marine calcifiers exhibit mixed responses to CO<sub>2</sub>-induced ocean acidification, *Geology*, 37, 1131–1134, 2009.
62. Ries, J. B., Ghazaleh, M. N., Connolly, B., Westfield, I., and Castillo, K. D.: Impacts of seawater saturation state ( $\Omega_{\text{A}} = 0.4\text{--}4.6$ ) and temperature (10, 25 °C) on the dissolution kinetics of whole-shell biogenic carbonates, *Geochimica et Cosmochimica Acta*, 192, 318–337, 2016.
63. Rollion-Bard, C., Blamart, D., Trebosc, J., Tricot, G., Mussi, A., and Cuif, J.-P.: Boron isotopes as pH proxy: A new look at boron speciation in deep-sea corals using <sup>11</sup>B MAS NMR and EELS, *Geochimica et cosmochimica acta*, 75, 1003–1012, 2011.
64. Sanyal, A., Bijma, J., Spero, H., and Lea, D. W.: Empirical relationship between pH and the boron isotopic composition of *Globigerinoides sacculifer*: Implications for the boron isotope paleo-pH proxy, *Paleoceanography*, 16, 515–519, 2001.
65. Saulnier, S., Rollion-Bard, C., Vigier, N., and Chaussidon, M.: Mg isotope fractionation during calcite precipitation: An experimental study, *Geochimica et Cosmochimica Acta*, 91, 75–91, 2012.
66. Schöne, B. R., Zhang, Z., Radermacher, P., Thébault, J., Jacob, D. E., Nunn, E. V., & Maurer, A. F. Sr/Ca and Mg/Ca ratios of ontogenetically old, long-lived bivalve shells (*Arctica islandica*) and their function as paleotemperature proxies. *Palaeogeography, palaeoclimatology, palaeoecology*, 302(1-2), 52-64, 2011.
67. Sillanpää, J. K., Ramesh, K., Melzner, F., Sundh, H., and Sundell, K.: Calcium mobilisation following shell damage in the Pacific oyster, *Crassostrea gigas*, *Marine Genomics*, 27, 75–83, 2016.



68. Sillanpää, J. K., Sundh, H., and Sundell, K. S.: Calcium transfer across the outer mantle epithelium in the Pacific oyster, *Crassostrea gigas*, *Proceedings of the Royal Society B: Biological Sciences*, 285, 20181676, 2018.
69. Sillanpää, J. K., Cardoso, J. C. dos R., Félix, R. C., Anjos, L., Power, D. M., and Sundell, K.: Dilution of seawater affects the  $\text{Ca}^{2+}$  transport in the outer mantle epithelium of *Crassostrea gigas*, *Frontiers in Physiology*, 11, 496427, 2020.
70. Stemmer, K., Brey, T., Gutbrod, M. S., Beutler, M., Schalkhausser, B., and De Beer, D.: In situ measurements of pH,  $\text{Ca}^{2+}$ , and DIC dynamics within the extrapallial fluid of the ocean quahog *Arctica islandica*, *Journal of Shellfish Research*, 38, 71–78, 2019.
71. Stewart-Sinclair, P. J., Last, K. S., Payne, B. L., and Wilding, T. A.: A global assessment of the vulnerability of shellfish aquaculture to climate change and ocean acidification, *Ecology and Evolution*, 10, 3518–3534, 2020.
72. Stoll, H., Langer, G., Shimizu, N., and Kanamaru, K.: B/Ca in coccoliths and relationship to calcification vesicle pH and dissolved inorganic carbon concentrations, *Geochimica et cosmochimica acta*, 80, 143–157, 2012.
73. Sutton, J. N., Liu, Y.-W., Ries, J. B., Guillermic, M., Ponzevera, E., and Eagle, R. A.:  $\delta^{11}\text{B}$  as monitor of calcification site pH in divergent marine calcifying organisms, *Biogeosciences*, 15, 1447–1467, 2018.
74. Thomsen, J., Casties, I., Pansch, C., Körtzinger, A., and Melzner, F.: Food availability outweighs ocean acidification effects in juvenile *Mytilus edulis* : laboratory and field experiments, *Global Change Biology*, 19, 1017–1027, 2013.
75. Ulrich, R. N., Guillermic, M., Campbell, J., Hakim, A., Han, R., Singh, S., Stewart, J. D., Román-Palacios, C., Carroll, H. M., and De Corte, I.: Patterns of element incorporation in calcium carbonate biominerals recapitulate phylogeny for a diverse range of marine calcifiers, *Frontiers in earth science*, 9, 641760, 2021.
76. Urey, H. C., Lowenstam, H. A., Epstein, S., and McKinney, C. R.: Measurement of paleotemperatures and temperatures of the Upper Cretaceous of England, Denmark, and the southeastern United States, *Geological Society of America Bulletin*, 62, 399–416, 1951.
77. Vogl, J., Rosner, M., and Pritzkow, W.: Development and validation of a single collector SF-ICPMS procedure for the determination of boron isotope ratios in water and food samples, *Journal of analytical atomic spectrometry*, 26, 861–869, 2011.
78. Waldbusser, G. G., Voigt, E. P., Bergschneider, H., Green, M. A., and Newell, R. I. E.: Biocalcification in the Eastern Oyster (*Crassostrea virginica*) in Relation to Long-term Trends in Chesapeake Bay pH, *Estuaries and Coasts*, 34, 221–231, 2011.
79. Waldbusser, G. G., Hales, B., Langdon, C. J., Haley, B. A., Schrader, P., Brunner, E. L., ... & Gimenez, I. Saturation-state sensitivity of marine bivalve larvae to ocean acidification. *Nature Climate Change*, 5(3), 273-280, 2015.
80. Wanamaker Jr, A. D., Kreutz, K. J., Wilson, T., Borns Jr, H. W., Introne, D. S., and Feindel, S.: Experimentally determined Mg/Ca and Sr/Ca ratios in juvenile bivalve calcite for *Mytilus edulis*: implications for paleotemperature reconstructions, *Geo-Marine Letters*, 28, 359–368, 2008.

81. Wang, B.-S., You, C.-F., Huang, K.-F., Wu, S.-F., Aggarwal, S. K., Chung, C.-H., and Lin, P.-Y.: Direct separation of boron from Na-and Ca-rich matrices by sublimation for stable isotope measurement by MC-ICP-MS, *Talanta*, 82, 1378–1384, 2010.
82. Wang, X., Wang, M., Jia, Z., Qiu, L., Wang, L., Zhang, A., and Song, L.: A Carbonic Anhydrase Serves as an Important Acid-Base Regulator in Pacific Oyster *Crassostrea gigas* Exposed to Elevated CO<sub>2</sub>: Implication for Physiological Responses of mollusc to Ocean Acidification, *Marine Biotechnology*, 19, 22–35, 2017.
83. Weiner, S., & Dove, P. M. . An overview of biomineralization processes and the problem of the vital effect. *Reviews in mineralogy and geochemistry*, 54(1), 1-29, 2003.
84. Wilbur, K. M., & Saleuddin, A. S. M. Shell formation. In *The mollusca* (pp. 235-287). Academic Press, 1983.
85. Wilbur, K. M. and Bernhardt, A. M.: Effects of amino acids, magnesium, and molluscan extrapallial fluid on crystallization of calcium carbonate: In vitro experiments, *The Biological Bulletin*, 166, 251–259, 1984.
86. Zeebe, R. E. and Wolf-Gladrow, D.: CO<sub>2</sub> in Seawater: Equilibrium, Kinetics, Isotopes, Gulf Professional Publishing, 382 pp., 2001.
87. Zhao, L., Milano, S., Walliser, E. O., and Schöne, B. R. Bivalve shell formation in a naturally CO<sub>2</sub>-enriched habitat: Unraveling the resilience mechanisms from elemental signatures, *Chemosphere*, 203, 132–138, 2018a.
88. Zhao, L., Milano, S., Tanaka, K., Liang, J., Deng, Y., Yang, F., Walliser, E.O., and Schöne, B. R. Trace elemental alterations of bivalve shells following transgenerational exposure to ocean acidification: Implications for geographical traceability and environmental reconstruction. *Science of the Total Environment*, 705, 135501, 2020.
89. Zittier, Z. M., Bock, C., Lannig, G., and Pörtner, H. O.: Impact of ocean acidification on thermal tolerance and acid–base regulation of *Mytilus edulis* (L.) from the North Sea, *Journal of experimental marine biology and ecology*, 473, 16–25, 2015.